SPIROCONJUGATION OVER A BORON ATOM: FACILE SYNTHESIS, STRUCTURES AND VIBRATIONAL SPECTRA OF CRYSTALLINE 1,3-DISUBSTITUTED (PROPEN-1,3-DIOLATO)(OXALATO)BORON MOLECULES

Panče Naumov[1], Minjas Zugik[2*], Albert Lee[3], Seik Weng Ng[3]

[1]*Osaka University, Graduate School of Engineering, Frontier Research Base for Global Young Researchers, 2-1 Yamada-oka, Suita, Osaka 565-0871, Japan*
[2]*Department of Physics, H. H. Wills Physics Laboratory, University of Bristol, Tyndall Avenue, Bristol, BS8 4TL, UK*
[3]*University of Malaya, 50603 Kuala Lumpur, Malaysia*
npance@wakate.frc.eng.osaka-u.ac.jp

Preparation of single crystals of spiroconjugated bis-chelated boron compounds containing ligands such as propen-1,3-diolates and oxalate, for application as lasing materials in dye laser technology, is burdened by their insolubility in organic solvents and the high melting temperatures. In this work, on the example of (diphenylpropen-1,3-diolato)(oxalato)boron (**1**) it is demonstrated that the solvothermal method can be successfully applied as facile, convenient and fairly inexpensive method to overcome the difficulties with preparation of such materials in single crystalline form directly from boric acid and the ligands. Solid-state IR spectra (recorded at room temperature and low temperature) and Raman spectra (recorded at room temperature) and equilibrium molecular geometries of **1** and three other disubstituted β-ketoboron molecules [RC(O)CHC(O)R'](O₂CCO₂)B (R = R' = *t*-butyl, **2**; R = methyl, R' = phenyl, **3**; R = R' = 2-pyridyl, **4**) in the ground electronic states were analyzed in detail, based on HF SCF (HF/3-21G, HF/6-31G), MP2 (MP2/6-31G) and DFT (B3LYP/6-31G) calculations. Minima with spiro-chelated tetrahedral (sp³) BO_4 or trigonal-planar (sp²) BO_3 coordination were located on the potential energy hypersurfaces for all systems. The tetrahedral structures are more stable relative to the trigonal structures (for example, ~37 kcal mol⁻¹ in the case of **2**), accounting for the observation that they represent the actual conformers in the solid state. Vibrational criteria for spectroscopic distinction between trigonal and tetrahedral boron–oxygen coordination geometry are presented.

Key words: *ab initio* calculations; boron; laser dyes; nonlinear materials; organoboron compounds; solvothermal synthesis; spiroconjugation; spirointeraction; vibrational spectra

СПИРОКОНЈУГАЦИЈА КАЈ АТОМ НА БОР: ЕФИКАСНА СИНТЕЗА, СТРУКТУРИ И ВИБРАЦИОНИ СПЕКТРИ НА КРИСТАЛНИ 1,3-ДИСУПСТИТУИРАНИ (ПРОПЕН-1,3-ДИОЛАТО)(ОКСАЛАТО)БОРНИ СОЕДИНЕНИЈА

Синтезата на монокристали на спироконјугирани бисхелатни борни соединенија со пропен-1,3-диолати и оксалат како лиганди, кои имаат примена во технологијата на ласерски бои, е отежната поради нивната слаба растворливост во органски растворувачи и високите температури на топење. Во овој труд, со (дифенилпропен-1,3-диолато)(оксалато)бор (**1**) како пример, е покажано дека солвотермичката синтеза може да се примени како ефикасен, корисен и прилично економичен метод за добивање на таквите материјали во форма на монокристали, и тоа директно од борна киселина и лигандите како реактанти. Врз основа на пресметки на HF SCF (HF/3-21G, HF/6-31G), MP2 (MP2/6-31G) и DFT (B3LYP/6-31G) ниво во основната електронска состојба, детално се анализирани инфрацрвените спектри во цврста фаза, снимени на собна температура и на ниска температура, раманските спектри снимени на собна температура, како и оптимизираните молекулски структури на **1** и три дисуп-

* Presently at CounterparyRisk Analytics, Citigroup London.

ституирани бета-кетоборни соединенија со формула [RC(O)CHC(O)R'](O₂CCO₂)B (R = R' = *terc*-бутил, **2**; R = метил, R' = фенил, **3**; R = R' = 2-пиридил, **4**). Кај енергетските хиперповршини на сите системи се лоцирани минимуми со спирохелатна тетраедарска (sp³) BO₄ и тригонално планарна (sp²) BO₃ координација. Во споредба со тригоналните структури, тетраедарските структури се релативно постабилни (на пример, за околу 37 kcal mol⁻¹ во случајот на **2**), што соодветствува со резултатот дека тоа се всушност конформери што постојат во цврста состојба. Образложени се и вибрационо-спектроскопски критериуми за претскажување на типот на координациска геометрија (тригонална или тетраедарска) кај бор-кислородни соединенија.

Клучни зборови: *ab initio* пресметки; бор, ласерски бои; нелинеарни материјали; органоборни соединенија; солвотермичка синтеза; спироконјугација; спироинтеракција; вибрациони спектри

1. INTRODUCTION

Organic colorants that are used in dye lasers [1] emit intense and coherent radiation upon laser excitation, either when dissolved in solvents or when incorporated into polymeric host matrices [2]. Such compounds usually show extensive electron delocalization in their molecular structures which permits efficient absorption of light from the near-ultraviolet to the visible region, followed by intense emission in the visible region. Four-coordinated boron compounds having two chelate ligands with π-systems oriented perpendicular to each other exhibit electron delocalization over the spiro boron atom termed *spirointeraction* (a term derived by analogy with the spiroconjugation at carbon atoms) which is responsible for the light emission of these compounds, in spite of absence of conventional π-bond resonance due to electron delocalization [3, 4]. An important example of spiroconjugated boron structure is the bis-chelated molecule (diphenylpropen-1,3-diolato)(oxalato)boron **1** (Chart 1) [5]. This material exhibits strong emission with amplified spontaneous emission spectra and high conversion efficiencies that are comparable or higher than the commercial dyes, and thus it represents a prototype structure for materials that can be used as lasing components [6]. Due to the insolubility in organic solvents and high melting points [7] of **1** and similar bis-chelated boron compounds containing propen-1,3-diolate and oxalate ligands, their structure determination has proved elusive, as all attempts to grow single crystals yielded only powders. From the (propen-1,3-diolato)(oxalato)boron compounds, only the structure of the 2,4-hexanedionato (R = Me, R' = Et in Chart 1) derivative has been determined [8]. On the other hand, the crystal structures of methyl- and phenyl-substituted (propen-1,3-diolato)boron mole cules having secondary ligands other than the oxalate are known for a number of mono- and bis-chelated compounds [9−13].

The absence of experimental data on the electronic, molecular and crystal structure of **1** and its notable lasing properties compared to other similar compounds prompted us to design a facile synthetic approach for preparation of this compound in single crystalline state, and to study the details of its equilibrium molecular structure by HF SCF and DFT calculations. To prepare **1** in single crystalline form we employed direct solvothermal synthesis from boric acid and the ligands, our efforts resulting in single crystals suitable for X-ray diffraction analysis. Furthermore, in order to provide information about the substitution effects, particularly of the extended electron conjugation with the phenyl rings in **1**, on the molecular and electronic structure of the (propen-1,3-diolato)(oxalato)boron skeleton, the structures and the vibrational spectra of the related molecules **2 − 4** in Chart 1 were calculated. Namely, it is known that the conjugation extent of bis-chelated boron−oxygen compounds similar to **1** determines the colour and therefore the absorption spectrum of the material, and can be tuned over a wide range of the wavelengths by proper choice of the substituents: alkyl-substituted compounds are usually colourless, mono- and diphenyl compounds are yellow, while the compounds having polycyclic aromatic substituents can be occasionally very intensely coloured.

1: R = R' = Ph

2: R = R' = t-butyl

**3:** R = Me, R' = Ph

4: R = R' = 2-pyridyl
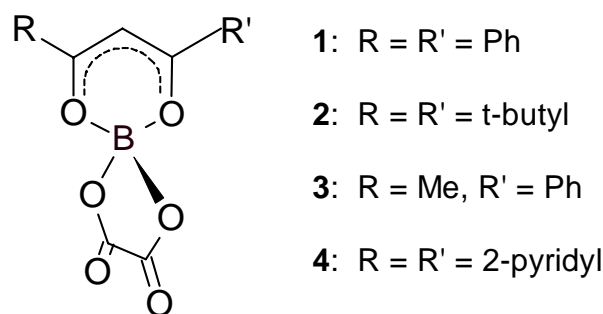
Chart. 1. Molecular structures of the (propen-1,3-diolato)(oxalato)boron compounds **1 – 4** studied in this work (Me and Ph stand for methyl and phenyl group, respectively)

2. EXPERIMENTAL

2.1. Synthesis and crystal structure analysis

Compounds **1 – 4** were synthesized in powder form according to Eq. 1, by melting mixtures of equimolar quantities of the respective diketone, oxalic acid dihydrate and boric acid. Excess of 1,2-dichloroethane was added to the melt to ensure complete dissolution.

$$RC(O)CH_2C(O)R' + B(OH)_3 + (COOH)_2 \cdot 2H_2O$$
$$\longrightarrow [RC(O)CHC(O)R'](O_2CCO_2)B + 5H_2O$$

(1)
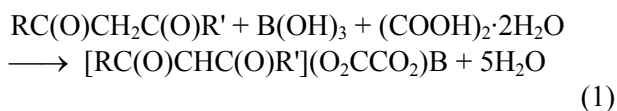
The products containing R = R' = *t*-butyl and R = R' = Ph (Ph denotes phenyl group) were obtained as powders after evaporation of the azeotropic mixture of the solvent and the water which appears as a product of the reaction. The derivatives containing R = Me, R' = Ph and R = R' = 2-pyridyl (Me stands for methyl group) were purified from toluene.

Single crystals of **1** were obtained by reacting dibenzoylmethane (0.22 g, 1 mmol), oxalic acid dihydrate (0.12 g, 1 mmol) and boric acid (0.06 g, 1 mmol) in toluene (10 mL) placed in a Teflon-lined stainless steel reactor (23 mL). The reactor was heated at 373 K for 3 days and allowed to cool slowly to room temperature. The solid product consisted of a mixture of colourless and yellow crystals and yellow powder material. A prismatic specimen (220 × 180 × 40 μm) of the yellow crystals was used in the diffraction measurements at 100 K. The details of the crystal structure determination and the respective references (CIF format) were deposited as Supporting Information.

2.2. Vibrational spectra

The FT IR spectra in the 10 000 – 370 cm^{-1} frequency range were recorded from pressed KBr pellets with a System 2000 FT IR spectrophotometer (Perkin–Elmer), by averaging 16 or 32 background and 32 or 64 sample spectra at resolution of 2 – 4 cm^{-1}. A P/N 21525 (Graseby Specac) variable-temperature cell equipped with KBr windows was used for both the room (RT) and liquid nitrogen boiling temperature (LNT) measurements. RT Raman spectra were recorded on a Renishaw Ramascope single dispersive instrument equipped with BH2-UMA microscope (Olympus) and air-cooled CCD camera. The 633 nm line of a He-Ne laser (Spectra Physics) was used for excitation. The entrance slit width was set to correspond to a resolution of 1 cm^{-1}. ν^4 dependence, Bose-Einstein, instrumental response and corrections due to the finite slitwidth to the Raman intensities were not performed. The Raman spectra were analyzed after correcting for the fluorescence-induced baseline (see below).

2.3. Calculations

Models of isolated

$[C_6H_5C(O)CHC(O)C_6H_5](O_2CCO_2)B$	**(1)**
$[(CH_3)_3CC(O)CHC(O)C(CH_3)_3](O_2CCO_2)B$	**(2)**
$[C_6H_5C(O)CHC(O)CH_3](O_2CCO_2)B$	**(3)**

and

$[CH_3C(O)CHC(O)C_2H_5](O_2CCO_2)B$	**(4)**
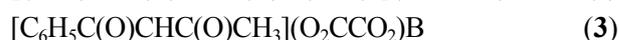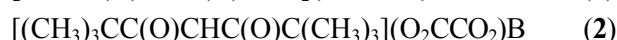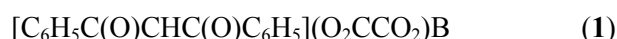
molecules were built [14] and initially optimized using the AM1 Hamiltonian [15, 16] The resulting structures were further optimized with the GAUSSIAN program suite [17, 18] and subsequently fully optimized in redundant internal coordinates employing the Berny algorithm [19–21] at the restricted Hartree-Fock level with the 3-21G basis set. Such level of computation was a compromise between accuracy and computer costs and was used only for comparative purposes of the isolated species in this study. There are indications that inclusion of polarization and diffuse functions to the basis set for molecules of a size as the ones treated here does not necessarily lead to improvement [22] and it may also cause some deterioration in the vibrational frequencies [23, 24]. On the other hand, only slight improvement in the frequencies might be gained (e.g., in respect to the matrix-isolated spectra) with the much more time-consuming DFT calculation [25, 26]. The electron correlation being of a special importance for the electronic structure and the lasing action of disubstituted (propen-1,3-diolato)(oxalato)boron molecules, further DFT calculations were performed using the B3LYP functional [27, 28] which accounts for the exchange and correlation effects, employing the larger 6-31G basis set. Separate MP2/6-31G [29] calculations were also performed. These two methods give better description of the electron delocalization and allow some assessment of the basis set extension. The equilibrium geometry of the derivative **1** containing phenyl groups obtained at the HF/3-21G level was further opti-

mised using these two higher theory level methods with the larger 6-31G basis set and additional single point energy calculations were performed on the other (propen-1,3-diolato)(oxalato)boron molecules.

Harmonic vibrational analysis on the equilibrium geometries of the above derivatives was performed by analytical computation of the second derivatives of the energy with respect to the Cartesian nuclear coordinates at the HF/3-21G level, yielding all real frequencies, respective infrared intensities and Raman scattering activities. To account for the basis set truncation, correlation effects (HF level) and vibrational anharmonicity, the neat frequencies were uniformly scaled by factor 0.9 [29]. This scaling scheme was applied in the same manner to all compounds for comparison with the experimental data. The relative partial charges were computed from the SCF density population analysis on the optimised geometries, employing the Mulliken partition scheme [30]. The computations were carried out partly on a PC and on workstations at TITech and the National Institute for Materials Science in Japan.

3. RESULTS AND DISCUSSION

3.1. Crystal structure of *1*

The molecule of **1** in the crystal lies on a two-fold rotation axis that passes through the boron atom, and through the midpoints of the oxalate groups. The boron atom is chelated by the oxalate group in a five-membered ring and by the dibenzoylmethane group in a six-membered ring (Fig. 1).
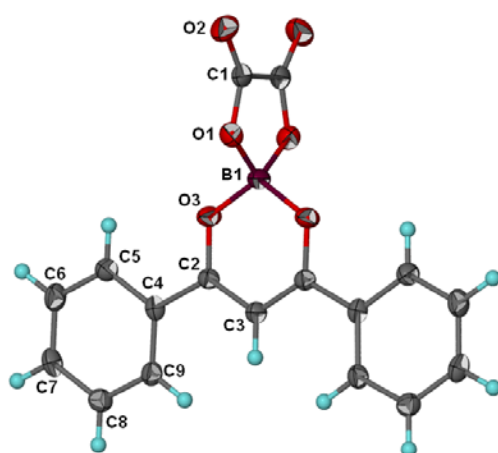

Fig. 1. Thermal ellipsoid plot of the molecular structure of [$C_6H_5C(O)CHC(O)C_6H_5$](O_2CCO_2)B (**1**)

The central feature of the molecule is the orthogornality of the two chelate rings, with interplanar angle of 88.8(1) °. The oxalate ligand exhibits single and double bonds, with respective distances of 1.325(2) and 1.193(2) Å. The C—O distances in the dibenzoylmethane ligand correspond to single bonds (1.311(2) Å). Consequently, the B—O distance is shorter when the oxygen atom belongs to the dibenzoylmethane group. The two B—O distances are significantly different: 1.477 (2) Å for the oxalate oxygen atom, and 1.457(2) Å in the case of the dibenzoylmethane oxygen atom. Inspection of the unit cell contents does not reveal any significant non-classical hydrogen bonds. On the other hand, the molecules are packed tightly in the unit cell, as noted from the relatively high density, which probably accounts for the insolubility in the common organic solvents.

3.2. Theoretical structures

The optimised geometries, Mulliken partial charges, dipole moments, energies, and vibrational frequencies for **1** − **4** are listed in Tables 1 − 6, atom labelling is shown in Chart 2. The HF/3-21G optimized molecular structures of **1** − **4** are shown in Fig. 2 and the theoretical and experimental vibrational spectra are presented in Figs. 4 − 6.
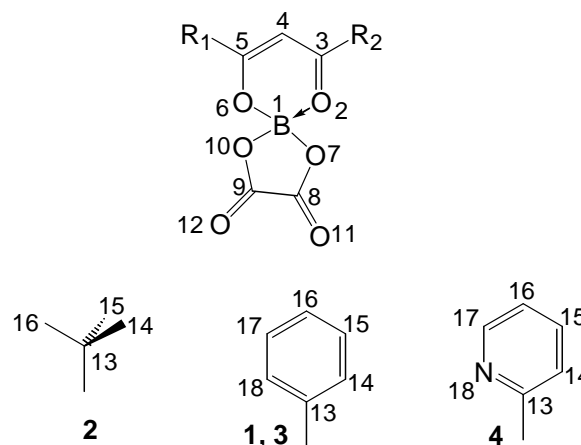
Chart. 2. Atom labelling of the studied (propen-1,3-diolato)(oxalato)boron molecules **1** – **4**

The input structure of the *t*-butyl derivative **2** for the HF/3-21G treatment was constructed by modifying the AM1 optimised structure of **1** and yielded a conformer with eclipsed *t*-butyl groups, one C−C bond of each butyl residue being in the plane of the (propen-1,3-diolato)boron ring (**2a**). Another AM1 minimum with a trigonal-planar co-

ordination of the boron was obtained starting from a model with *trans*-positioned *t*-butyl substituents with respect to the C4−C5 bond. This prompted us to examine this minimum further as well, and the output structure is denoted **2b** (Fig. 2). For the asymmetrically substituted molecule **3**, the two possible starting AM1 resonance forms,

$$[C_6H_5C(=O)CH=C(O)CH_3](O_2CCO_2)B$$

and

$$[C_6H_5C(O)=CHC(=O)CH_3](O_2CCO_2)B,$$
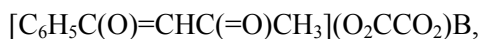
were considered; as expected, they ultimately converged to the same minimum. In the case of **4**, the three possible relative orientations of the 2-pyridine rings coplanar with the six-membered ring were HF/3-21G optimized. The energy minimization of one of the mirror forms resulted in rotation of the second pyridyl ring around the C5−C13 bond, revealing that this isomer represents a high-energy local minimum, and thus only two stereoisomers were ultimately obtained (**4a** and **4b**). The C_2 symmetric isomer (**4b**, Fig. 2) is about 9.44 kcal mol^{-1} (HF/3-21G//HF/3-21G) more stable form in the gas phase.

3.2.1. Equilibrium geometries of 1 − 4. The structure of **2b** is radically different from the other compounds, and therefore will be discussed separately. Aside of **2b**, all symmetrically substituted (propen-1,3-diolato)(oxalato)boron compounds have C_{2v} molecular point symmetry (Fig. 2, Tables 1 and 2). The molecular structures of the studied compounds consist of planar and perpendicular to one another propen-1,3-diolato and oxalato rings bridged by a spiro-type boron atom. Therefore, the boron atom is placed in tetrahedral BO$_4$ environment found in a number of boron−oxygen coordination compounds [8, 12, 31, 32]. The electron delocalization stabilizes coplanarity of the substituent phenyl and pyridine rings with the propen-1,3-diolato chelate ring in all cases.

Except for somewhat shorter C3−O2 bond in **4a**, the geometry of the propen-1,3-diolato ring is similar in all compounds. The C3−O2 and C5−O6 bonds are elongated from their ketone values upon coordination, except for **4a**, they are nearly equally long, revealing extensive electron delocalization within the coordination ring. The theoretical C3−O2 and C5−O6 distances compare very well those in the crystals of bisacetato(acetylacetonato)boron, (**5**, 1.296(4) Å) [12] and (ethylmethylpropen-1,3-diolato)(oxalato)boron (**6**, 1.296(5) and 1.309(6) Å) [8]. The C4−C5 and C3−C4 bond

lengths are clearly dependent on the substituent: they are equal in case of symmetric substitution (**1**, **2** and **4b**) and are similar to the average value in **5** (1.362(4) Å) [12], **6** (1.364(8) and 1.360(6) Å) [8] and in (acetylacetonato)diphenylboron (**7**, 1.381 (2) Å) [13], but different in case of antisymmetric substitution or orientation (**3** and **4a**). The bond length difference, therefore, depends on the electronic effects expressed by the substituents *via* the type (comparison between **1** and **4b**, **2** and **4b**) and orientation (comparison between **4a** and **4b**) of the substituents. The oxalate geometry is preserved constant in all compounds and is identical with the previously reported structures. The coordinated oxalate C−O bonds (1.349 Å) are elongated more than those of the propen-1,3-diolate fragment (*cca.* 1.302 Å), which accounts, in addition to the chelation strain, for the shortening of the other two oxalate C=O bonds (1.190 Å) compared to the usual values. Although the bond angles are somewhat more sensitive to substitution, most of the angles show variation of less than 3° in the studied compounds.

The theoretical B−O bond lengths (*cca.* 1.49 and 1.46 Å) agree well with the solid-state average value (1.477(5) Å) obtained from various esters of diarylboronic acids [33−35], but are larger than those (1.438(5) Å) reported for the dimeric 2-salicylideneaminoethanol derivatives of the phenylboronic acid with BO$_2$NPh coordination [36]. The theoretical B−O values from the diphenylpropen-1,3-diolato ring in **1** are similar to those in the planar chelate rings of **5** (1.471(4) Å [12]) and (benzoylacetonato)difluoroboron, **8** (1.488(3) Å [37]), but different than in the B-envelope distorted ring in **7** (1.538(7) Å [13]), which shows reliability of the current theoretical HF method in prediction of the real values. Correspondence with the B−O distances in the solid **6** is also apparent (1.454(4), 1.483(6) Å; 1.466(5), 1.450(7) Å [8]). The internal ring angles at the boron atom are rather constant (about 106.2 and 104.0 °) and, as in the known structures, the BO$_4$ tetrahedron is only slightly distorted. The deviation from 120 ° on the side of the larger chelate ring is compensated with somewhat larger internal angles at O2 and O6.

The internal bond angles reveal some strain in the oxalate−boron ring; nonetheless, the planarity is preserved and extensive electron delocalization occurs. The aromatic substituents are planar within the calculation errors. No significant deviations were found in the structure of the aromatic

phenyl and pyridine rings. The *t*-butyl groups substituents in **2a** are distorted by elongation of one C−C bond. The calculations, moreover, reveal that electronic factors rather than packing effects (which are not included in the calculations) can

account for the unexpectedly short C−CH₃ bond in the methyl analogue **3** (calculated: 1.493 Å) that was noted previously in the crystal structures of **7** (1.489(6) Å) [13] and at low temperature in **8** (1.485(3) Å) [37].
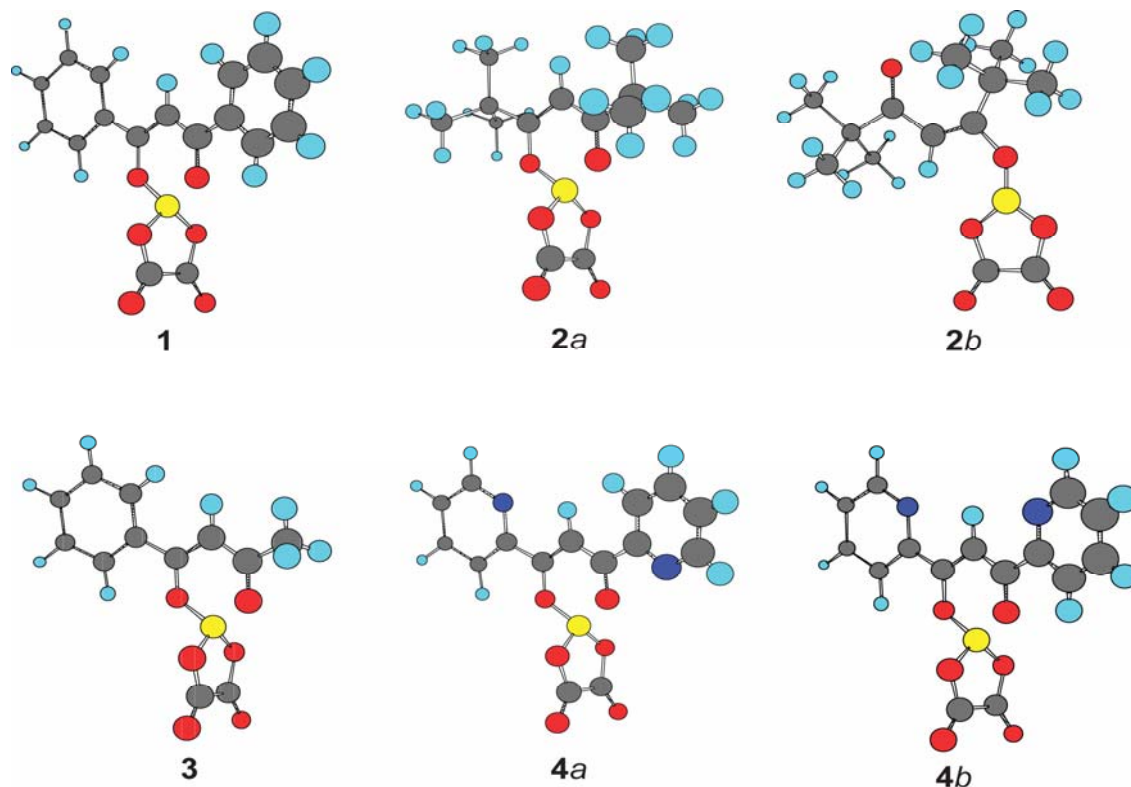

Fig. 2. *Ab initio* (HF/3-21G) optimized molecular structures of [C₆H₅C(O)CHC(O)C₆H₅](O₂CCO₂)B (**1**), [(CH₃)₃CC(O)CHC(O)C(CH₃)₃](O₂CCO₂)B, (**2**) [C₆H₅C(O)CHC(O)CH₃](O₂CCO₂)B (**3**) and [CH₃C(O)CHC(O)C₂H₅](O₂CCO₂)B (**4**) (*a* and *b* refer to different isomers obtained from various starting geometries)

T a b l e 1

Relative Mulliken partial atomic charges, absolute energies and dipole moments for the substituted (propen-1,3-diolato)(oxalato)boron molecules[a]

Atom[b]	Compound[c]					
	1	**2a**[d]	**2b**[d]	**3**[e]	**4a**[d]	**4b**[d]
(Propen–1,3–diolato)(oxalato)boron skeleton						
B1	1.330	1.329	1.291	1.330	1.328	1.327
O2	−0.796	−0.775	−0.600	−0.790	−0.762	−0.796
C3	0.639	0.702	0.637	0.656	0.625	0.582
C4	−0.115	−0.172	−0.136	−0.149	−0.057	0.008
C5	0.639	0.702	0.573	0.557	0.582	0.583
O6	−0.796	−0.775	−0.778	−0.760	−0.796	−0.796
Sum[f]	**−0.429**	**−0.318**	**−0.304**	**−0.486**	**−0.408**	**−0.419**
Oxalate						
O7	−0.769	−0.771	−0.733	−0.769	−0.768	−0.769
C8	0.779	0.779	0.778	0.779	0.780	0.778
C9	0.779	0.779	0.781	0.779	0.780	0.778
O10	−0.769	−0.771	−0.759	−0.769	−0.768	−0.769
O11	−0.557	−0.556	−0.502	−0.555	−0.557	−0.556
O12	−0.557	−0.556	−0.502	−0.555	−0.557	−0.556
Sum	**−1.094**	**−1.096**	**−0.937**	**−1.090**	**−1.090**	**−1.094**

Atom[b]	Compound[c]					
	1	**2a**[d]	**2b**[d]	**3**[e]	**4a**[d]	**4b**[d]
Substituents[g]						
C13	–0.197	–0.380	–0.379	–0.206	0.257	0.249
C14	0.056	0.157	0.135	0.150	0.111	0.110
C15	0.018	0.157	0.116	0.021	0.091	0.088
C16	0.053	0.107	0.116	0.057	–0.037	–0.037
C17	0.020			0.019	0.395	0.395
C18	0.147			0.062		
N18					–0.724	–0.713
C13'		–0.380	–0.378	0.144	0.238	0.249
C14'		0.157	0.107		0.045	0.110
C15'		0.157	0.107		0.089	0.088
C16'		0.107	0.126		–0.035	–0.037
C17'	0.020				0.398	0.395
C18'	0.147					
N18'					–0.660	–0.713
Energies[h]						
$E / 10^5$ kcal mol^{-1}	–7.013785	–6.097380	–6.096927	–5.825330	–7.213380	–7.213474
Dipole moments						
μ / D	13.123	12.104	1.701	12.861	14.320	11.173

[a] The charges of the hydrogens were summed up into the respective heavy atoms.

[b] The labels refer to Chart 2. Primed atoms refer to the second substituent in the symmetric compounds.

[c] Numbers stand for [C₆H₅C(O)CHC(O)C₆H₅](O₂CCO₂)B (**1**), [(CH₃)₃CC(O)CHC(O)C(CH₃)₃](O₂CCO₂)B (**2**)
  [C₆H₅C(O)CHC(O)CH₃](O₂CCO₂)B (**3**) and [CH₃C(O)CHC(O)C₂H₅](O₂CCO₂)B (**4**).

[d] Forms *a* and *b* correspond to the two possible stereoizomers of **4** obtained from the energy minimizations (see text).

[e] For this unsymmetrical derivative, the C5 and C3 in Chart 2 are bound to the methyl C13' and phenyl C13 atoms, respectively (the labelling of
  the phenyl ring is the same as for **1**).

[f] Excluding the boron atom.

[g] The parameters in the same line *do not* necessarily correspond to the same parameter. For the meaning of the labels in each case see Chart 2.

[h] Sum of the electronic and zero-point energies.

T a b l e 2

Ab initio structural parameters of the (propen-1,3-diolato)(oxalato)boron part in the substituted (propen-1,3-diolato)(oxalato)boron molecules[a]

Parameter[b]	Compound[c]							
	1			**2a**[d]	**2b**[d]	**3**[e]	**4a**[d]	**4b**[d]
	HF[f]	B3LYP[g]	MP2[h]					
B1–O2	1.492	1.500	1.527	1.493		1.500	1.496	1.495
O2–C3	1.304	1.333	1.343	1.301	1.220	1.300	1.291	1.303
C3–C4	1.383	1.398	1.407	1.382	1.473	1.390	1.384	1.376
C4–C5	1.383	1.398	1.407	1.382	1.329	1.373	1.373	1.376
C5–O6	1.304	1.333	1.343	1.301	1.409	1.302	1.301	1.303
O6–B1	1.492	1.500	1.527	1.493	1.339	1.491	1.499	1.495
B1–O7	1.459	1.478	1.492	1.458	1.407	1.457	1.456	1.458
O7–C8	1.349	1.377	1.398	1.349	1.371	1.349	1.349	1.349
C8–C9	1.541	1.542	1.553	1.541	1.539	1.541	1.541	1.541
C9–O10	1.349	1.377	1.398	1.349	1.376	1.349	1.349	1.349
O10–B1	1.459	1.478	1.492	1.458	1.414	1.457	1.456	1.458
C8–O11	1.190	1.220	1.239	1.19	1.183	1.190	1.190	1.190
C9–O12	1.190	1.220	1.239	1.19	1.182	1.190	1.190	1.190
C4–H	1.060	1.076	1.083	1.06	1.066	1.062	1.061	1.061
O2–B1–O6	106.2	109.0	108.8	106.1		106.2	106.0	106.3
O2–B1–O10	111.7	110.6	110.4	111.7		111.4	111.8	111.7
B1–O2–C3	126.8	125.2	124.7	126.7		127.4	127.3	126.0
O2–C3–C4	120.5	120.1	120.7	120.7	124.3	119.9	120.7	122.0
C3–C4–C5	119.1	120.4	120.4	118.9	129.4	118.7	118.1	117.7
C4–C5–O6	120.5	120.1	120.7	120.7	116.9	122.0	122.3	122.0
C5–O6–B1	126.8	125.2	124.7	126.7	136.6	125.9	125.5	126.0
O7–B1–O10	103.9	105.5	106.3	104.0	107.5	104.1	104.2	103.9
B1–O7–C8	111.8	110.1	109.4	111.7	110.8	111.7	111.6	111.8

Parameter[b]	Compound[c]						
	1			**2a**[d]	**2b**[d]	**3**[e]	**4a**[d]	**4b**[d]
	HF[f]	B3LYP[g]	MP2[h]					
O7–C8–C9	106.3	107.1	107.4	106.3	105.7	106.3	106.3	106.3
C8–C9–O10	106.3	107.1	107.4	106.3	105.4	106.3	106.3	106.3
C9–O10–B1	111.8	110.1	109.4	111.7	110.6	111.7	111.6	111.8
O7–C8–O11	126.7	125.7	125.6	126.7	126.4	126.7	126.7	126.7
O10–C9–O12	126.7	125.7	125.6	126.7	125.9	126.7	126.7	126.7

[a] Distances in Ångströms, angles in degrees.

[b] Labels refer to Chart 2. Primed atoms Refer to the second substituent in the symmetric compounds.

[c] Numbers stand for $[C_6H_5C(O)CHC(O)C_6H_5](O_2CCO_2)B$ (**1**), $[(CH_3)_3CC(O)CHC(O)C(CH_3)_3](O_2CCO_2)B$ (**2**)
$[C_6H_5C(O)CHC(O)CH_3](O_2CCO_2)B$ (**3**) and $[CH_3C(O)CHC(O)C_2H_5](O_2CCO_2)B$ (**4**).

[d] Forms *a* and *b* correspond to the two possible stereoizomers of **4** obtained from the energy minimizations (see text). Calculations were performed at the HF/3-21G level.

[e] For this unsymmetrical derivative, the C5 and C3 in Chart 2 are bound to the methyl C13' and phenyl C13 atoms, respectively. Calculations were performed at the HF/3-21G level.

[f] HF/3-21G.

[g] B3LYP/6-31G.

[h] MP2/6-31G.

Table 3

Ab initio (HF/3-21G) structural parameters of the substituents in the substituted
(propen-1,3-diolato)(oxalato)boron molecules[a]

Parameter[b]	Compound[c]					
	1	**2a**[d]	**2b**[d]	**3**[e]	**4a**[d]	**4b**[d]
C5–C13	1.467	1.510	1.531		1.470	1.468
C5–13'				1.493		
C3–C13				1.464		
C3–C13'	1.467	1.510	1.532		1.478	1.468
C13–C14	1.392	1.548	1.547	1.391	1.380	1.380
C13–C15		1.548	1.547			
C13–C16		1.535	1.542			
C13'–C14'	1.392	1.548	1.545		1.384	1.380
C13'–C15'		1.548	1.545			
C13'–C16'		1.535	1.537			
C14–C15	1.379			1.380	1.386	1.385
C15–C16	1.386			1.384	1.381	1.381
C16–C17	1.383			1.387	1.388	1.389
C17–C18	1.380			1.379		
C17–N18					1.323	1.322
C13–C18	1.391			1.393		
C13–N18					1.330	1.330
C14'–C15'	1.379				1.384	1.385
C15'–C16'	1.386				1.381	1.381
C16'–C17'	1.383				1.386	1.389
C17'–C18'	1.380					
C17'–N18'					1.323	1.322
C13'–C18'	1.391					
C13'–N18'					1.329	1.330
C5–C13–C16		112.8	110.7			
C5–C13–C14		107.2	109.4		120.3	120.3
C5–C13–C15		107.2	109.4			
C16–C13–C14		110.0	108.4			
C16–C13–C15		110.0	108.4			
C14–C13–C15		109.4	110.5			
C3–C13'–C16'		112.8	108.9			
C3–C13'–C14'		107.2	109.6			
C3–C13'–C15'		107.2	109.6			
C16'–C13'–C14'		110.0	109.2			

Parameter[b]	Compound[c]					
	1	2a[d]	2b[d]	3[e]	4a[d]	4b[d]
C16'–C13'–C15'		110.0	109.2			
C14'–C13'–C15'		109.4	110.2			
C13–C14–C15	120.2			120.2	118.1	118.1
C14–C15–C16	120.0			119.9	119.0	119.0
C15–C16–C17	120.2			120.2	118.9	118.9
C16–C17–C18	119.9			120.0		
C16–C17–N18					121.9	121.9
C17–C18–C13	120.2			120.1		
C17–N18–C13					119.3	119.3
C14–C13–C18	119.5			119.6		
C14–C13–N18					106.0	122.7
C13'–C14'–C15'	120.2				118.6	118.1
C14'–C15'–C16'	120.0				119.1	119.0
C15'–C16'–C17'	120.2				118.6	118.9
C16'–C17'–C18'	119.9					
C16'–C17'–N18'					122.0	121.9
C17'–C18'–C13'	120.2					
C17'–N18'–C13'					119.8	119.3
C14'–C13'–C18'	119.5					
C14'–C13'–N18'					121.9	122.7

[a] Distances in Ångströms, angles in degrees.

[b] The parameters in the same line *do not* necessarily correspond to the same parameter. For the meaning of the labels in each case see Chart 2. Primed atoms refer to the second substituent in the symmetric compounds.

[c] Numbers stand for $[C_6H_5C(O)CHC(O)C_6H_5](O_2CCO_2)B$ (**1**), $[(CH_3)_3CCOCHCOC(CH_3)_3](O_2CCO_2)B$ (**2**) $[C_6H_5C(O)CHC(O)CH_3](O_2CCO_2)B$ (**3**) and $[CH_3C(O)CHC(O)C_2H_5](O_2CCO_2)B$ (**4**).

[d] Forms *a* and *b* correspond to the two possible stereoizomers of **4** obtained from the energy minimizations (see text).

[e] For this unsymmetrical derivative, the C5 and C3 in Chart 2 are bound to the methyl C13' and phenyl C13 atoms, respectively (the labelling of the phenyl ring is the same as for **1**).

Contrary to **2a**, the molecular structure of **2b** features trigonal-planar coordination of the boron with –C(*t*-buty)=O rotated around the C3–C4 bond (Fig. 2), which leads to *trans*-positioned O6 and O2 with respect to C4–C5. The DFT single point calculations characterized this isomer far less stable in the gas phase, the RB+HF-LYP//HF energy difference with the tetragonal isomer **2a** being 37.34 kcal mol^{-1}. In **2b**, the coordinated oxygen atoms are coplanar, and also coplanar with the oxalate and *trans*-propen-1,3-diolato parts and the butyl C16 and C16' atoms, forming the molecular mirror plane, whereas the oxalate ring is asymmetric. The sp^2 hybridized boron in **2b** features all B–O bonds shorter than the respective counterparts of the sp^3 boron in **2a** (Table 2). This is transferred to some extent to the oxalate *exo*-carbonyl groups, while the uncoordinated C3=O2 bond exhibits normal double bond length. As the resonance over the boron atom is no longer possible, the C3–C4 and C4–C5 bonds (1.382 Å in **2a**) become different (1.473 and 1.329 Å, respectively). The structure **2b** may further involve a short C4–H···O2 contact since the proton here is alkene-type, the oxygen atom is notably negative (–0.759) and the equilibrium geometry seems suit-able for such interaction (H···O2 = 2.23 Å, C4–H···O2 = 120.4°).

In principle, the presence of the conformer *b* of **2** in the solid state, i.e. trigonal boron coordination and thus absence of spirointeraction could be considered as one of the possible reasons behind the absence of colour in this compound. It seems that existence of such potential minimum is likely in absence of aromatic rings in either of the C3 and C5 atoms, which through electronic effects (e.g. resonance) would otherwise stabilize the tetrahedral isomer **2a**. The trigonal coordination does not seem to be a result of *intrinsic* molecular geometrical factors: the structure of **2a**, namely, features no exceptional bond parameters from the other compounds (Table 2) and there are no apparent steric constraints for the substituents in this case. Instead, the reasons of such structural preference are either in the intermolecular forces, or most probably in the electronic interaction with the aromatic substituent (Table 1), as mentioned above. These presumptions fit well the colour exhibited by the (propen-1,3-diolato)(oxalato)boron compounds: the aromatic-ring containing compounds **1**, **3** and **4** are coloured, while **2**, in which such resonance stabilization is not possible, is colour-

less. These presumptions, however, are not supported by the large potential energy of the local trigonal coordination minimum. Another strong argument against such straightforward inference about the coordination type comes from the (methylethylpropen-1,3-diolato)(oxalato)boron, which is a colourless solid, but again comprises a single type tetrahedrally coordinated boron atoms [8].

Additional semiempirical calculations were performed to examine the possibility of trigonal boron coordination in **1**, **3** and **4**. Unlike in **2***b*, in the high-energy trigonal minimum of **1**, the rigidity of the substituents severely strains the B1−O6−C5(C13)=C4−C3(O)−C13' part from planarity; the phenyl rings are nearly perpendicular to each other. The side-chains are distorted from planarity in the trigonal minima of the other compounds as well (Fig. 3). As these high-energy geometrical isomers are less likely to occur and are not of interest for the goals of this study, they were not examined any further.
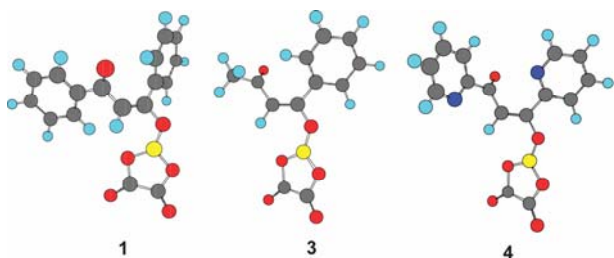
Fig. 3. Structures with trigonal-planar coordination of the boron obtained by geometry optimizations of [$C_6H_5C(O)CHC(O)C_6H_5$](O_2CCO_2)B (**1**), [$C_6H_5C(O)CHC(O)CH_3$](O_2CCO_2)B (**3**) and [$CH_3C(O)CHC(O)C_2H_5$](O_2CCO_2)B (**4**).

3.2.2. Comparison of the theoretical methods. DFT/B3LYP/6-31G geometry optimisations produced the tetrahedral isomer of **1**. All bonds lengths predicted at this theory level in the case of **1** are longer than those obtained at HF/3-21G, the average difference being 0.020 Å. The inclusion of the electron correlation *via* the DFT method affects all bonds within the spiro-structure, and is mostly reflected in lengthening of the endo C−O bonds for *cca*. 0.03 Å in both chelate rings, but does not have any significant effect on the lengths of the exo carbonyl groups and oxalate C−C bond. The influence on the internal angles is small with the average at 1.3 °. The MP2/6-31G method also predicts all bonds longer in the basal structure than the HF calculations and also similar angles (average: 0.035 Å, 1.5 °). Interestingly, the lengthening

is especially pronounced in all carbonyl groups of the oxalate part (around 0.05 Å), and then in the propen-1,3-diolato C−O lengths. The above analysis shows that accounting for the electron correlation effects (with a larger basis set) generally produces larger size of the chelate structure, and therefore represent the real bond lengths.

3.3. Mulliken partial charges

Except for **2***b*, **3** and **4***a* that lack a two-fold symmetry axis, the charge is distributed symmetrically with respect to the oxalate plane (Table 1). The charge variations within the propen-1,3-diolato ring caused by different substituents are neither reflected in the charge of the boron, nor transferred to the oxalate part of the complex. The coordinated oxygen atoms carry the largest negative charges in both rings, but the oxalate oxygens are slightly less charged. According to the present partition scheme, the charges of all coordinated oxygen atoms are closest to one another in case of **2**. Less negatively charged than the coordinated oxygen atoms (about −0.8) are the terminal oxalato oxygen atoms (about −0.56). A positive charge always resides on the substitution carbon atoms; this is on the account of C4, which may be negative or slightly positive. Except for the large negative charge on the nitrogen atoms in **4***a* and **4***b*, the values on all substituent atoms are relatively small. Summation of charges within the two coordination rings excluding the joint atom reveals that while the oxalate part carries similar charge in all studied systems, that of the propen-1,3-diolato part varies considerably and is closest in value with the former in **2**. The charge analysis implies quantitative differences between the electronic structure of **2** and the other studied boron compounds, which may be one of the factors for the absence of colour in case of the former.

3.4. Infrared spectra

3.4.1. General discussion. As in the case with the similar compounds **5** − **7** [8, 12, 13], stronger intermolecular interactions than the usual van der Waals contacts are not expected in the solids of **1** − **4**, which is confirmed by the structure determination of **1** (see above). Although the absence of hydrogen bonding in the studied systems improves the theoretical prediction of the experimental spec-

tra, the harmonic approximation of isolated molecular entities in gas phase is a crude description of the polycrystalline, solid state, anharmonic vibrational data. Nevertheless, Figs. 4 and 5 and Table 4 exhibit rather good resemblance between the scaled HF/3-21G theoretical and the experimental spectra of the solid samples. The mean deviation between the two is within the range expected from similar calculations on small organic molecules

[38]. Deviations of the computed frequencies at the uncorrelated HF level when compared to experiment in absence of polarisation and diffuse functions, is *a priori* expected for the frequencies of the out-of-plane ring modes [39, 40], which appear regularly as very weak bands and can hardly be assigned with confidence in the solid-state spectra without additional techniques.

T a b l e 4

Ab initio (HF/3-21G) theoretical and experimental vibrational data for the substituted (propen-1,3-diolato)(oxalato)boron molecules[a]

No	Experimental frequencies of **1** / cm^{-1}		Theoretical frequencies of **1** and **2** / cm^{-1}						Approximate Description of the modes of **1**[c]
	IR	Raman	**1**	**2a**	**2b**	**1**[b]	**2a**[b]	**2b**[b]	
1	3141		3512	3512	3444	3161	3161	3100	$\nu(C^4H)$
2	3117		3426	3311	3351	3083	2980	3016	$\nu(C^{18}H),\nu(C^{17}H)$
3	3117		3426	3511	3349	3083	3160	3014	$\nu(C^{18}H),\nu(C^{17}H)$
4			3403	3306	3288	3063	2975	2959	$\nu(C^{14}H),\nu(C^{15}H),\nu(C^{16}H)$
5			3401	3306	3288	3061	2975	2959	$\nu(C^{14}H),\nu(C^{15}H),\nu(C^{16}H),\nu(C^4H)$
6	3087		3389	3274	3279	3050	2947	2951	$\nu(CH^{Ph})$
7	3087		3389	3273	3275	3050	2946	2948	$\nu(CH^{Ph})$
8	3068		3378	3267	3273	3040	2940	2946	$\nu(CH^{Ph})$
9	3068		3378	3267	3270	3040	2940	2943	$\nu(CH^{Ph})$
10	3050		3364	3265	3260	3028	2939	2934	$\nu(C^{15}H),\nu(C^{16}H),\nu(C^{17}H)$
11	3050		3364	3265	3259	3028	2939	2933	$\nu(C^{15}H),\nu(C^{16}H),\nu(C^{17}H)$
12	1826 1811		2053	3263	3256	1848	2937	2930	$\nu_{ip}(C^8O^{11}C^9O^{12})$
13	1779		2026	3263	3253	1823	2937	2928	$\nu_{op}(C^8O^{11}C^9O^{12})$
14			1771	3211	3219	1594	2890	2897	$\nu(CC^{Ph}),\delta(CH^{Ph})$
15	1601		1771	3211	3214	1594	2890	2893	$\nu(CC^{Ph}),\delta(CH^{Ph})$
16	1589 1585		1756	3206	3205	1580	2885	2885	$\nu(CC^{Ph}),\delta(CH^{Ph}),\nu(C^5O^6),\nu(C^3O^2)$
17	1554sh		1749	3206	3202	1574	2885	2882	$\nu(CC^{Ph}),\delta(CH^{Ph}),\delta(C^4H)$
18	1551 1547		1685	3201	3202	1517	2881	2882	$\nu(C^3C^4),\nu(C^4C^5),\delta(C^4H),\delta(CH^{Ph})$
19	1523		1682	3201	3200	1514	2881	2880	$\nu(CC^{Ph}), \delta(CH^{Ph}),\nu(C^5O^6),\nu(C^3O^2)$
20	1500		1667	2054	2082	1500	1849	**1874**	$\nu(CC^{Ph}),\delta(CH^{Ph}),\nu(C^5O^6),\nu(C^3O^2)$
21	1494 1487		1659	2027	2056	1493	1824	1850	$\nu(CC^{Ph}),\delta(CH^{Ph}),\nu(C^3C^4),\nu(C^4C^5)$
22	1462sh		1626	1697	1890	1463	1527	1701	$\nu(CC^{Ph}),\delta(CH^{Ph}),\delta(CCC^{Ph})$
23	1442		1603	1696	1791	1443	1526	1612	$\nu(CC^{Ph}),\delta(CCC^{Ph}),\delta(CH^{Ph}),\nu(C^5O^6),\nu(C^3O^2)$
24	1361		1512	1678	1705	1361	1510	1535	$\delta(CH^{Ph}),\delta(C^{13`}C^5C^4),\delta(C^{13}C^3C^4)$

No	Experimental frequencies of **1** / cm^{-1}		Theoretical frequencies of **1** and **2** / cm^{-1}						Approximate Description of the modes of **1**[c]
	IR	Raman	**1**	**2a**	**2b**	**1**[b]	**2a**[b]	**2b**[b]	
25	1335 1330		1509	1678	1691	1358	1510	1522	$\delta(CCC^{Ph}),\delta(CH^{Ph}),\delta(C^4C^3O^2),\delta(C^4C^5O^6)$
26	1319 1312		1484	1678	1687	1336	1510	1518	$\nu(C^5C^{13}),\nu(C^3C^{13'}),\delta(C^4C^3O^2),$ $\delta(C^4C^5O^6),\nu(CC^{Ph})$
27	1299		1460	1677	1680	**1314**	1509	1512	$\nu(C^3C^4),\nu(C^4C^5),\delta(CH^{Ph}),\nu(C^5O^6),$ $\nu(C^3O^2),\delta(CH^{Ph})*$
28			1369	1672	1679	1232	1505	1511	$\delta(CH^{Ph}),\delta(C^4H),\delta(C^4C^3O^2),\delta(C^4C^5O^6)$
29	1247		1367	1671	1676	1230	1504	1508	$\delta(C^4H),\delta(CH^{Ph})$
30	1257		1358	1663	1672	1222	1497	1505	$\delta(C^4H),\delta(CH^{Ph}),\delta(C^4H),$
31	1208		1344	1662	1663	1210	1496	1497	$\delta(CH^{Ph})$
32	1198		1338	1658	1657	1204	1492	1491	$\delta(CH^{Ph})$
33	1171 1111 1098		1333	1657	1655	1200	1491	1490	$\nu(C^8C^9),\delta(CH^{Ph}),\delta(C^8C^9O^{12}),\delta(C^9C^8O^{11})$
34	1117? 1111		1294	1651	1655	**1165**	1486	1490	$\nu_{as}(B^1O_4),\delta(CH^{Ph})*$
35	1098		1288	1651	1653	**1159**	1486	1488	$\nu_{op}(B^1O^7O^{10}),\nu(B^1O^7),\nu(B^1O^{10})*$
36	1078		1264	1600	1647	1138	1440	**1482**	$\nu(CC^{Ph}),\delta(CH^{Ph})$
37	1051		1258	1598	1611	**1132**	1438	1450	$\nu(CC^{Ph}),\nu_{as}(B^1O_4)*$
38	1068sh		1233	1571	1599	1110	1414	1439	$\delta(C^4H),\delta(C^{14}C^{13}C^{18}),$ $\delta(C^{14'}C^{13'}C^{18'}),\nu(C^5O^6),\nu(C^3O^2)$
39			1207	1570	1589	1086	1413	1430	$\nu(CC^{Ph}),\delta(CH^{Ph})$
40			1206	1567	1573	1085	1410	1416	$\gamma(CH^{Ph})$
41			1206	1567	1571	1085	1410	1414	$\gamma(CH^{Ph})$
42	1068sh?		1199	1468	1571	1079	**1321**	1414	$\delta(CH^{Ph}),\delta(C^4H)$
43			1191	1467	1565	1072	1320	1409	$\nu(CC^{Ph}),\delta(C^4C^5O^6),\delta(C^4C^3O^2),\delta(CCC^{Ph})$
44			1173	1401	1407	1056	1261	1266	$\gamma(CH^{Ph})$
45			1172	1373	1385	1055	1236	1247	$\gamma(CH^{Ph})$
46	998		1137	1354	1364	1023	1219	1228	$\delta(CH^{Ph})$
47	972		1137	1344	1361	1023	**1210**	1225	$\delta(CH^{Ph})$
48	956		1130	1342	1347	**1017**	1208	**1212**	$\nu_{op}(B^1O^7O^{10}),\nu(C^8O^7),\nu(C^9O^{10}),\gamma(CH^{Ph})*$
49			1125	1340	1346	1013	1206	1211	$\gamma(CH^{Ph})$
50			1122	1319	1342	1010	**1187**	1208	$\gamma(CH^{Ph})$
51			1111	1295	1301	1000	**1166**	**1171**	$\delta(CCC^{Ph})$
52			1106	1294	1237	995	1165	1113	$\delta(CCC^{Ph}),\delta(C^3C^4C^5)$
53			1063	1288	1198	957	**1159**	1078	$\delta(C^3C^4C^5),\delta(B^1O^2C^3),\delta(B^1O^6C^5),\nu(CC^{Ph})$
54	824? 812?		1048	1178	1186	943	1060	1067	$\gamma(C^4H),\gamma(CH^{Ph}),\gamma(C^3C^4C^5)$
55			990	1176	1177	891	1058	1059	$\gamma(CH^{Ph})$
56			988	1170	1166	889	1053	1049	$\gamma(CH^{Ph})$
57			984	1168	1140	**886**	1051	1026	$\nu_{op}(B^1O^2O^6),\nu(C^3C^4),\nu(C^4C^5)*$

No	Experimental frequencies of **1** / cm^{-1}		Theoretical frequencies of **1** and **2** / cm^{-1}						Approximate Description of the modes of **1**^{c}
	IR	Raman	**1**	**2a**	**2b**	**1**^{b}	**2a**^{b}	**2b**^{b}	
58			966	1131	1106	**869**	**1018**	995	$\nu_s(B^1O_4), \nu(C^8C^9), \delta(C^4C^3O^2), \delta(C^4C^5O^6), \delta(C^3C^4C^5)*$
59			936	1094	1095	842	985	986	$\gamma(CH^{Ph}), \gamma(C^4C^3O^2), \gamma(C^4C^5O^6)$
60			924	1094	1091	832	985	**982**	$\gamma(O^7C^8C^9), \gamma(O^{10}C^9C^8)$
61	779		898	1082	1086	808	**974**	977	$\gamma(CH^{Ph}), \gamma(C^4H)$
62			874	1045	1052	787	941	**947**	Skeletal def. of the Ph$_2$-propen-1,3-diolato part
63	760		828	1039	1028	745	935	925	$\gamma(C^4H), \gamma(CH^{Ph})$
64			820	1032	1021	738	929	919	$\delta(O^2B^1O^6), \nu(C^8C^9), \delta(CCC^{Ph})$
65			803	1016	1020	723	914	918	$\gamma(CH^{Ph}), \gamma(C^4C^3O^2), \gamma(C^4C^5O^6)$
66	720		789	991	1018	710	892	916	$\gamma(CH^{Ph}), \gamma(C^4H)$
67			774	977	962	697	**879**	**866**	$\gamma(CCC^{Ph}), \gamma(C^4C^3O^2), \gamma(C^4C^5O^6)$
68			773	965	922	696	**869**	830	$\delta(B^1O^7O^{10}), \nu(C^8C^9)$
69	680		735	936	903	**662**	**842**	813	$\gamma(O^2B^1O^6), \delta(C^8O^{11}), \delta(C^9O^{12}), \gamma(C^4H)*$
70			717	924	861	**645**	832	775	Skeletal def. of the Ph$_2$-propen-1,3-diolato part *
71	635		709	887	839	638	798	755	$\delta(CCC^{Ph})$
72			707	880	790	636	792	711	$\delta(CCC^{Ph}), \delta(B^1O^2C^3), \delta(B^1O^6C^5)$
73	610		677	827	750	**609**	744	**675**	Skeletal def. of the Ph$_2$-propen-1,3-diolato part *
74			652	786	748	**587**	707	673	$\delta(O^7C^8C^9), \delta(O^8C^9O^{10})*$
75	569		633	783	715	**570**	705	**644**	Skeletal def. of the Ph$_2$-propen-1,3-diolato part *
76			536	759	713	482	**683**	**642**	$\gamma(CCC^{Ph}), \gamma(C^3C^4C^5)$
77	458		527	738	688	**474**	**664**	**619**	$\gamma(C^8O^{11}), \gamma(C^9O^{12}), \gamma(O^7C^8C^9), \gamma(C^8C^9O^{10})*$
78			503	652	655	453	**587**	**590**	$\gamma(CH^{Ph}), \gamma(CCC)$
79			465	633	635	419	**570**	572	$\gamma(CCC^{Ph})$
80			464	576	541	418	518	487	$\gamma(CCC^{Ph})$
81			461	545	524	415	491	472	$\delta(C^3O^2B^1), \delta(C^5O^6B^1)$, Ph-ring rocking
82			438	530	511	**394**	477	**460**	Skeletal*
83			388	497	481	**349**	447	433	$\gamma(O^2B^1O^6)$, skeletal*
84			368	444	428	331	**400**	385	$\delta_s(O^{11}C^8C^9O^{12})$
85			343	436	422	309	392	380	$\gamma(B^1O^7C^8), \gamma(B^1O^{10}C^9), \gamma(B^1O^2C^3), \gamma(B^1O^6C^5)$
86			296	408	414	266	367	373	Skeletal
87			293	392	389	264	353	350	Skeletal
88			261	390	366	235	351	329	"Breathing"
89			235	373	363	212	336	327	$\gamma(CCC^{Ph}), \gamma(C^3C^4C^5)$
90			208	368	357	187	331	321	$\gamma(B^1O^7C^8), \gamma(B^1O^{10}C^9), \gamma(CCC^{Ph})$
91			185	364	354	**167**	328	319	Skeletal *
92			134	348	328	121	313	295	$\gamma(B^1O^7C^8), \gamma(B^1O^{10}C^9), \gamma(CCC^{Ph}), \gamma(C^4CO)$
93			89	347	307	80	312	276	Skeletal
94			84	327	304	76	294	274	Ph-ring rocking

No	Experimental frequencies of **1** / cm^{-1}		Theoretical frequencies of **1** and **2** / cm^{-1}						Approximate Description of the modes of **1**^{c}
	IR	Raman	**1**	**2a**	**2b**	**1**^{b}	**2a**^{b}	**2b**^{b}	
95			61	324	295	55	292	266	Oxalate ring twisting
96			46	311	284	41	280	256	Oxalate ring wagging
97			38	294	269	34	265	242	Skeletal
98			25	285	252	23	257	227	Ph-ring librations
99			23	282	241	21	254	217	Ph-ring librations
100				268	239		241	215	
101				260	200		234	180	
102				243	196		219	176	
103				216	180		**194**	**162**	
104				148	165		133	149	
105				134	142		121	128	
106				127	100		114	90	
107				66	53		59	48	
108				52	49		47	44	
109				46	37		41	33	
110				35	24		32	22	
111				25	16		23	14	

^{a} The frequencies in the same line *do not* necessarily correspond to the same mode. The labels **1** – **4** refer to Chart 2.

^{b} Empirically scaled with the scaling factor 0.9. Modes that involve significant displacement of the boron atom are bolded.

^{c} Symbols denote: ν – stretching, δ – in-plane bending, γ – out-of-plane bending ip – in-phase, op – out-of-phase, as – antisymmetric, s – symmetric, Ph – phenyl. Modes that involve significant displacement of the boron atom are marked with asterisks. The atom labels refer to Chart 2.

^{d} Oxalate ring librations.
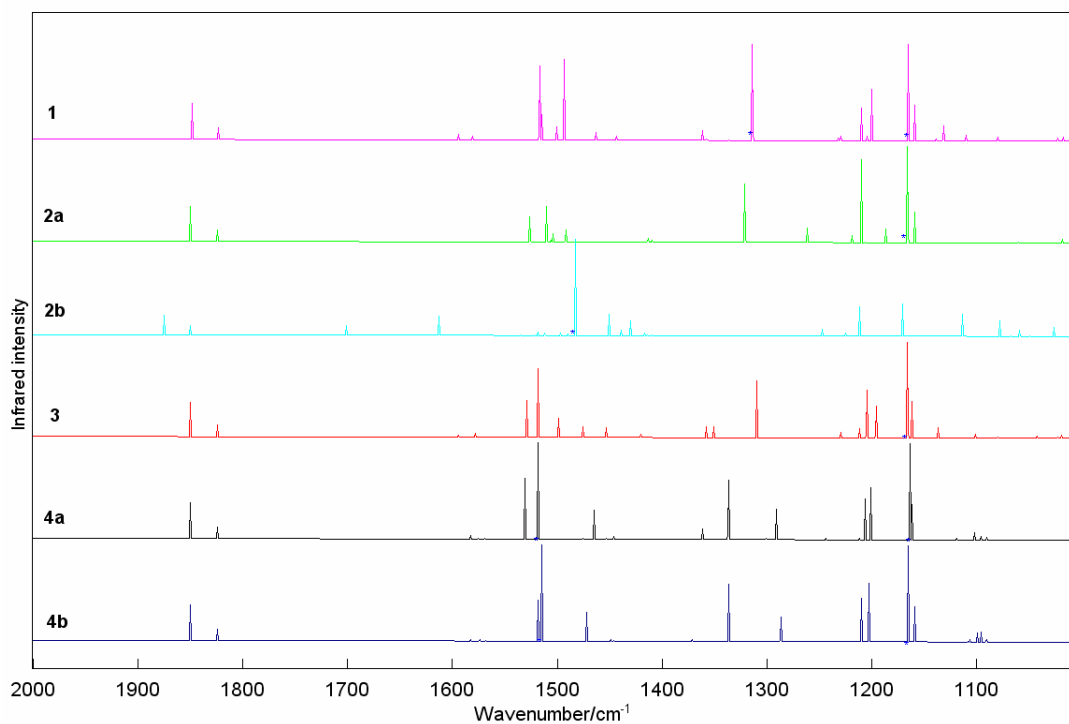
Fig. 4. The 2000 – 1000 cm^{-1} region of the theoretical IR spectra (HF/3-21G) of [RC(O)CHC(O)R'](O$_2$CCO$_2$)B. R = R' = phenyl (**1**); R = R' = *t*-butyl with tetrahedral (**2b**) and trigonal (**2b**) coordination of the boron; R = methyl, R' = phenyl (**3**); R = R' = 2-pyridyl (**4**) (**4b** is the C$_2$ symmetric isomer). For convenience, nine strongest bands are shown with limited intensity and are denoted with asterisks. Frequencies are uniformly scaled with 0.9.
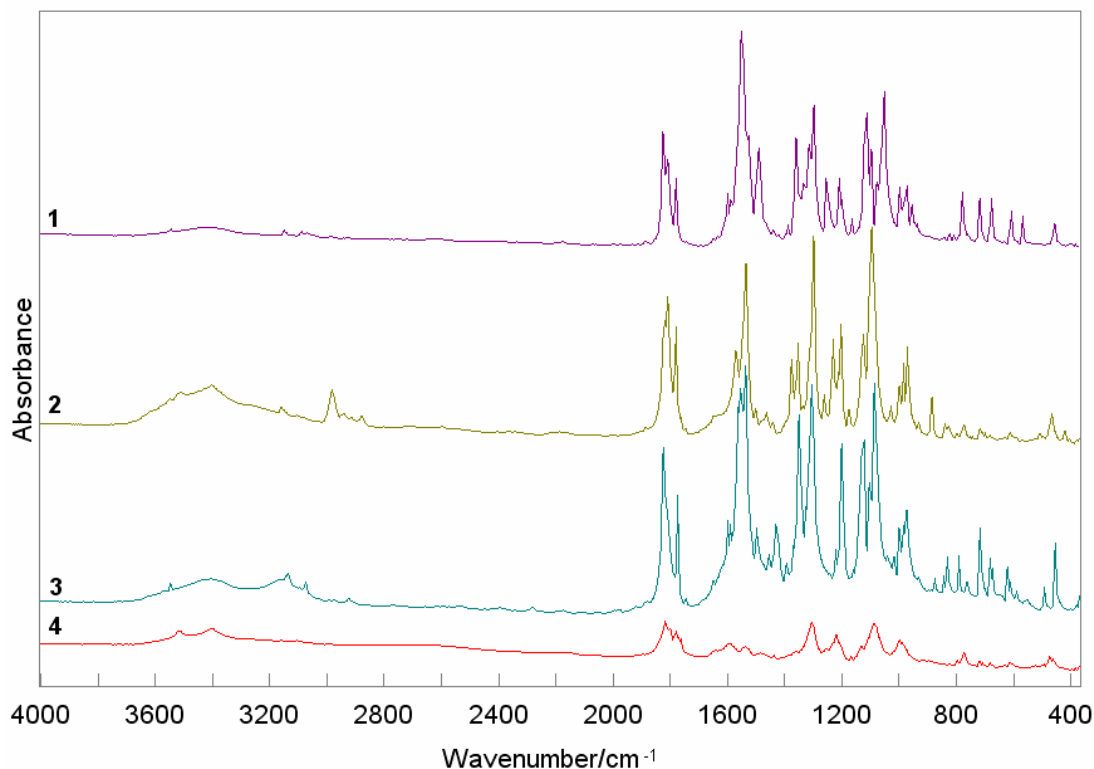
Fig. 5. The 2000 − 370 cm^{-1} region in the solid-state FT IR spectra of [RC(O)CHC(O)R'](O$_2$CCO$_2$)B. R = R' = phenyl (**1**); R = R'= *t*-butyl (**2**); R = methyl, R' = phenyl (**3**), and R = R' = 2-pyridyl (**4**).

3.4.2. Spectral assignments. The scaled HF/3-21G vibrational data for **1** and **2** and the band assignments of the spectrum of **1** are listed in Table 4. The discrepancy between the experimental and theoretical data is especially pronounced for the CH stretches and the modes below 1000 cm^{-1}. In what follows, the spectrum of molecule **1** will be discussed, with occasional reference to those of the other compounds.

The assignment of the ν(CH) stretchings is straightforward, as these are the only fundamentals of this system to be found in the 3250 − 2830 cm^{-1} region. The highest frequency fundamental band of **1** owes to practically pure ν(C4H) mode, being followed by several overlapped aromatic stretches. The frequency of the ν(C4H) Raman band for a vinyl-type CH should be lowered for nearly 70 cm^{-1} in **2***b* in respect to the highest-frequency ν(CH) modes of **1**, **2***a* and **4**, and about 37 cm^{-1} from **3**.

Bands from the stretchings of the uncoordinated oxalate CO groups (ν$_{12}$ and ν$_{13}$) are found apart from the other fundamentals in the 1860 − 1755 cm^{-1} region. These modes were reported at 1825 and 1785 cm^{-1} in the spectrum of the methylethyl analogue **6** [8]. Three prominent mostly Lor-

entzian-type bands in the IR spectra of **1**, **2** and **3**, and at least seven overlapped bands in **4** were resolved by spectral reconstruction (Table 5), indicating more than one type of oxalate residues in the last case. Except for **4**, the similar intensity within the triplet and the small value of the theoretical frequency difference may indicate that the larger number of bands is a consequence of vibrational splitting due to the solid-state effects on the spectra. The calculations predict ν$_{ip}$ (ν$_{12}$) > ν$_{op}$ (ν$_{13}$) frequency order, inherent for the electronic structure of the bidentate oxalate anion, with a ν$_{ip}$−ν$_{op}$ difference of about 25 cm^{-1} and larger intensities of the in-phase mode (ν$_{12}$) in both the IR and Raman spectra. Reversed order of the ν$_{ip}$ and ν$_{op}$ carbonyl frequencies ν$_{ip}$ < ν$_{op}$ and IR intensities are known from the spectra of other small-sized cyclic dicarbonyl compounds, e.g. the cyclic imides [41, 42]. Bearing in mind the fundamental difference in the physical state between the models and experiment, the fair similarity of the intensity ratio (ν$_{Band I}$ + ν$_{Band II}$) / ν$_{Band III}$ from Table 5 and that predicted for ν$_{12}$ / ν$_{13}$ (typically 75 / 25), suggests that the higher frequency doublet might originate from the in-phase −C8(=O11)C9(=O12)− stretching (ν$_{12}$).

T a b l e 5

Curve-fitting results for the oxalate ν (OCCO)
region of the infrared spectra[a]

Band I			Band II			Band III
Compound **1**						
1826			1811			1779
35.6			*46.1*			*18.2*
(0.89)			(0.37)			(1.00)
Compound **2**						
1823			1809			1779
28.4			*53.2*			*18.4*
(1.00)			(1.00)			(1.00)
Compound **3**						
1824			1810			1775
37.7			*49.5*			*12.9*
(1.00)			(1.00)			(1.00)
Compound **4**						
1829	1819	1810	1800	1788	1778	1763
30.6	*19.0*	*3.6*	*12.4*	*3.3*	*20.8*	*10.2*
(0.30)	(1.00)	(1.00)	(0.08)	(0.00)	(1.00)	(1.00)

[a] The (experimental) frequencies are given in cm^{-1}. Integrated
intensities (normalized to the sum of 100 %) are in italic. The
numbers in brackets represent the Lorentzian function contribution
to the band shapes.

A group of overlapped IR bands with varying
intensities originating from the highly coupled
phenyl (ν_{14}–ν_{17}, ν_{19}–ν_{23}) and C3C4C5 backbone
(ν_{18}) stretchings appears between 1620 and
1460 cm^{-1}.

A quadruplet of intense modes ν_{18}–ν_{21} with
close frequencies appears as a strong complex
strong absorption in the 1580 – 1505 cm^{-1} region,
featuring at least three maxima and several shoul-
ders. The bands of the pyridyl analogue (**4**) in this
region are split better and, correspondingly, far
less intense.

Modes consisted mostly of CH, CCC and
CCO deformations give rise to bands at frequen-
cies lower than 1400 cm^{-1}. The prominent bands
around 1360 and 1300 cm^{-1} (predicted at 1361 and
1314 cm^{-1}), correspond to mixed δ(CH) (ν_{24}) and
ν(C3C4)/ν(C4C5) (ν_{27}) modes, respectively, the
latter including significant displacement of the
boron atom. The in-plane CH deformations
(ν_{28}–ν_{32}) appear in the 1265–1160 cm^{-1} region,
while the out-of-plane modes give rise to very
weak IR bands (except for ν_{54}, ν_{61} and ν_{66}, **1**) be-
low 1000 cm^{-1}.

The most intense band in the IR spectrum of
1 should correspond to the antisymmetric stretch-
ing of the BO$_4$ tetrahedron, ν_{34}, predicted at about
1165 cm^{-1} for all tetrahedral models. This mode
appears as a prominent band at 1085 and
1088 cm^{-1} in the spectra of **3** and **4**, respectively,
whereas doublets (1117, 1111 cm^{-1} and 1099,
1120 cm^{-1}) are present in the spectra of **1** and **2**
(see below). This mode was previously reported as
a B−O stretching at 1370 cm^{-1} in the spectrum of
tetrahedral **6** [8]. As the most intense, BO$_4$ breath-
ing Raman mode in **1** appears at 1380 cm^{-1}, the IR
band at 1370 cm^{-1} probably corresponds to the
symmetric stretching mode.

3.4.3. Vibrational discrimination between
BO$_4$ and BO$_3$ coordination. The substantially dif-
ferent point symmetry of **2**a and **2**b should be well
reflected in the respective vibrational spectra, and
especially in the modes localized in the coordina-
tion polyhedron; such vibrations, moreover, should
be detectable within the frequency range in this
study. A general characteristic apparent from
Fig. 5 is the pronounced similarity of the IR spec-
trum of **2** with **1** and **3** (in **4**, as mentioned before,
probably several molecular types exist, and thus
the complicated spectral appearance is understand-
able). This is the first indication that these struc-
tures should comprise the same chelating unit.

Assignments of the ν(BO) modes are known
in wide frequency range; a brief outline of such
results will be presented in continuation. Distor-
tion of the D_3 borate ion to C_s in the aragonite-type
borates results in infrared activation of the totally
symmetric ν(BO$_3$) mode at 939 cm^{-1} [36]. The re-
spective mode in C_{3h} boric acid at 880 cm^{-1} is only
Raman active [43]. The antisymmetric mode in the
acid and the alcoxyborates has been usually found
around 1430 cm^{-1} [44]. *Ab initio* calculations at
the RHF/6-31+G(d,p) level recently assigned the
BO symmetric stretchings of the metaborate ring
[B$_3$O$_6$]$^{3-}$ in molten BaB$_2$O$_4$ and CsBO$_2$ at (1460,
630 cm^{-1}) and (1503, 606 cm^{-1}), respectively [45].
The types of borate networks in borate glass matri-
ces are semi-quantitatively discriminated by use of
their Raman spectra [46, 47]. The strong band at
806 cm^{-1} is representative for the totally symmet-
ric breathing mode of the boroxol rings; inclusion
of alkali oxides and the change of the boron coor-
dination sp^2 → sp^3 shifts the band to ~795 cm^{-1},
giving rise to another one at ~770 cm^{-1}. Similarly,
the two crystal modifications of K$_2$O-5B$_2$O$_3$ featur-
ing pentaborate moieties and thus both three- and

tetracoordinated boron atoms, show absorptions at 885 and 765, and 925 and 785 cm^{-1} [46, 47]. A band in a very narrow interval 964–968 cm^{-1} in the spectra of alkali dipinacol hydrates is characteristic for the tetrahedrally coordinated boron [48]. B–O stretching frequencies as high as 1907.5 cm^{-1} are known from the laser-ablation products of boron and methanol isolated in cryogenic argon matrices.[49] The type of boron coordination can be independently assessed by the ^{11}B shifts in the NMR spectra: δ values about +5 ppm are expected for tetracoordination, while +25 − 28 ppm are expected for tricoordination. Hence, in addition to giving complete *ab initio* vibrational assignment for **1** and comparison with the other studied boronates, the other goal of the present vibrational analysis was to screen, on theoretical grounds, for suitable frequency region(s) indicative for the boron coordination type in the (propen-1,3-diolato)(oxalato)boron systems.

The distinct symmetry of the two equilibrium structures of **2** results in substantially different theoretical vibrational spectra (Table 4, Fig. 4). From 111 fundamental modes of the tetrahedral **2a**, 16 involve significant displacement of the boron atom (Table 6, denoted ν_{42}^a, ν_{47}^a, ν_{50}^a, ν_{51}^a, ν_{53}^a, ν_{58}^a, ν_{61}^a, ν_{67}^a−ν_{69}^a, ν_{76}^a−ν_{79}^a, ν_{84}^a, ν_{103}^a for **2a**), while 14 such modes were detected for trigonal planar **2b** (ν_{20}^b, ν_{36}^b, ν_{48}^b, ν_{51}^b, ν_{60}^b, ν_{62}^b, ν_{67}^b, ν_{73}^b, ν_{75}^b−ν_{78}^b, ν_{82}^b, ν_{103}^b) (the oxalate ring librations also involve boron displacement; these, however, were not accounted for). Excluding weak modes, band couples ν_{47}^a/ν_{48}^b, ν_{51}^a/ν_{51}^b and ν_{58}^a/ν_{67}^b are not reliable for distinction as they should appear with similar intensity at close frequencies in both types of coordination. Despite these, *six* prominent infrared bands remain indicative: for the spectrum of the tetrahedral **2a**, bands at 1321 (strong, ν_{42}^a), 1187 (medium, ν_{50}^a) and 1159 (strong, ν_{53}^a) are characteristic, while for the trigonal planar **2b**, those at 1874 (strong, ν_{20}^b), 1482 (very strong, ν_{36}^b) and 642 (medium, ν_{76}^b; all values scaled with 0.90). Two Raman bands in addition are specific for the spectrum of **2b**: 1874 (medium, ν_{20}^b) and 1482 (weak to medium, ν_{36}^b).

Expected frequency lowering of $\nu_{ip}(C^8O^{11}C^9O^{12})$ (ν_{20}) and $\nu_{op}(C^8O^{11}C^9O^{12})$ (ν_{21}) for about 20 and 17 cm^{-1} for the form *b* of **2** from the other boron compounds is not observed in the IR spectra; instead, band positions are in the frequency range of the other boronates and support the existence of isomer *a* (Fig. 5).

T a b l e 6

Vibrational modes of the boron coordination in the two isomers of (di-t-butylpropen-1,3-diolato)(oxalato)boron

2a				**2b**			
Mode	Freq.^{a}	IR^b	R^b	Mode	Freq.^{a}	IR^b	R^b
				ν_{20}^b	1874	s	m
				ν_{36}^b	1482	vs	wm
ν_{42}^a	1321	s	vw				
				ν_{48}^b	1212	s	vw
ν_{47}^a	1210	s	w				
ν_{50}^a	1187	m	vw				
				ν_{51}^b	1171	s	vw
ν_{51}^a	1166	vs	vw				
ν_{53}^a	1159	s	vw				
ν_{58}^a	1018	m	vw				
				ν_{60}^b	982	vw	vw
ν_{61}^a	974	vw	w				
				ν_{62}^b	947	w	vw
ν_{67}^a	879	w	vw				
ν_{68}^a	869	vw	vw				
				ν_{67}^b	866	m	vw
ν_{69}^a	842	w	vw				
ν_{76}^a	683	vw	vw				
				ν_{73}^b	675	vw	w
ν_{77}^a	664	vw	-				
				ν_{75}^b	644	vw	vw
				ν_{76}^b	642	m	-
				ν_{77}^b	619	vw	vw
				ν_{78}^b	590	vw	vw
ν_{78}^a	587	vw	vw				
ν_{79}^a	570	vw	vw				
				ν_{82}^b	460	w	vw
ν_{84}^a	400	w	vw				
ν_{103}^a	194	vw	vw				
				ν_{103}^b	162	vw	vw

^{a} Theoretical (HF/3-21G) frequency
^{b} Symbols denote: s – strong, vs – very strong, m – medium, wm – weak to medium, w – weak, vw – very weak.

The strong ν_{42} band (coupled $\nu(C3C4C5)$ stretching) expected around 1321 cm^{-1} (1314 cm^{-1} for **1**) appears at 1300 cm^{-1}. This band may be the equivalent of the band at 1370 cm^{-1} in the spectrum of the tetrahedral (ethylmethylpropen-1,3-diolato)(oxalato)boron, that was formerly empiri-

cally assigned as B−O stretching [8]. There is little doubt that this band originates from any mode of the isomer *b*, as no strong bands for the latter are expected in the region 1439 – 1225 cm^{-1}. The $\nu_{51}{}^{a}$ mode expected at around 1166 cm^{-1}, which represents the asymmetric stretching of the BO_4 tetrahedron, corresponds to the doublet of the strongest bands in the spectrum of **2** at 1099 and 1094 cm^{-1}; this represents the strongest evidence for the tetrahedral coordination in the *t*-butyl analogue. Similar bands are also observed for all other studied systems (**1**, 1051 cm^{-1}; **3**, 1085 cm^{-1}; **4**, 1088 cm^{-1}). The frequency order of the modes ν_{50} and ν_{51} of **2** is inverted in respect to the corresponding modes ν_{34} and ν_{35} of **1**, and thus ν_{51} is preceded by the out-of-phase $B^1O^7O^{10}$ stretching mode (ν_{50}) at 1127 cm^{-1}. The latter band, however, is not very prominent and characteristic, and may be also a result of some of the modes $\nu_{51}{}^{b}$−$\nu_{53}{}^{b}$. The strongest band in the IR spectrum of **2b** should be the $\nu_{36}{}^{b}$ mode (1482 cm^{-1}, Fig. 4), almost 4.5 times more intense than the second strongest one ($\nu_{51}{}^{b}$, 1171 cm^{-1}). Although the exact relative HF intensities are not reliable for quantitative comparison with the experimental data, there is no such prominent band in the IR spectrum of **2**; instead, the most prominent bands feature similar intensity, as expected for **2a**. The presence of medium strong IR bands lower than the strongest doublet 1099/1094 cm^{-1} does not coincide with the calculations that for **2a** predict only weak bands below 1159 cm^{-1} ($\nu_{53}{}^{a}$). Series of such bands with gradually descending intensities are expected for the isomer **2b**; nevertheless, groups of similar bands below 1000 cm^{-1} are also found in the spectra of the other boron compounds and are due to infrared activation of the weak modes in this region. In fact, except for the butyl librations, the spectral appearance of **2** in the lower IR region is very similar with that of **1**, and no band could be assigned to the mode ν_{76} of **2b** around 642 cm^{-1}.

From the above discussion, it can be concluded about presence of the isomer *a* in the solid state of the (di-*t*-butylpropen-1,3-diolato)(oxalato)-boron, as in the diphenyl, methyl-phenyl and pyridyl-pyridyl analogues. The spectrum of the latter, however, can not be assigned with confidence, but it is likely that a mixture of rotational isomers exist. The experimental polycrystalline spectra of the studied systems are rather complex and future matrix isolation or solution studies should contribute more accurate assignments. The

absolute values of the frequencies in the present case, especially of the lower-frequency modes, largely depend on the scaling scheme used, and, therefore, can not be rigorously relied on for coordination prediction. The HF method, on the other hand, does not provide representative quantitative picture of the relative intensities, which additionally complicates the assignment.

3.5. Raman spectra and normal modes of *1* and *2*

Due to fluorescence the bands in the Raman spectra of **1** and **2** are superimposed on an intense and sloping baseline (Fig. 6). The Raman bands were obtained after fitting a sixth order function to the baseline and subsequently subtracting it from the total observed spectrum (Fig. 7). To a first approximation **1** can be regarded as possessing C_{2v} point symmetry and the normal vibrations should transform in the same way as irreducible representations of the C_{2v} point group. **1** is a 35 atom molecule and the total number of normal modes is 99. The vibrational irreducible representation of **1** is $\Gamma_{vib} = 34A_1 + 15A_2 + 20B_1 + 30B_2$. All modes are active in Raman and A_2 modes are inactive in IR. The molecule **1** can be "broken up" into several parts and the normal vibrations of these parts will be separately discussed (of course bearing in mind that the modes of the individual parts of the molecule are coupled). In the case of **1**, the vibrational irreducible representation can be broken up as follows: (1) normal vibrations of the phenyl rings, (2) vibrations of the propen-1,3-diolato ring, (3) modes of the BO_4 pseudo-tetrahedron, (4) modes of the oxalate ring. Immediately follows that the phenyl C−C skeletal modes are coupled with the C−C modes of the propendiolato ring of **1**, the C−O modes of the propendiolato ring with the modes of the BO_4 tetrahedron, and the modes of BO_4 are directly influenced by the modes of the oxalate ring of **1**. The symmetry of **1** also causes modes of the "left" (above) and of the "right" (below) parts of the molecule to vibrate in-phase and out-of-phase with each and each mode consequently is split in two components. For example the in-phase stretching modes belong to the A_1 species, and the out-of-phase modes to B_2 (B_1) species.

The highest frequency bands in the Raman spectrum are due to vinyl and aromatic CH stretching modes. Since there is only one vinyl C−H group in the molecule, **1** should give rise only to one band of very small intensity in the Raman

spectrum and it appears at round 3150 cm^{-1}. The IR counterpart of this mode has a bit larger intensity. HF/3-21G level of theory fails very badly in predicting the relative Raman C−H intensities; they are predicted to be much more intense than they actually are in the spectrum of **1**. The reasons behind this are the low level of theory and the usage of frequency-independent polarisabilities in the computation of the Raman intensities.
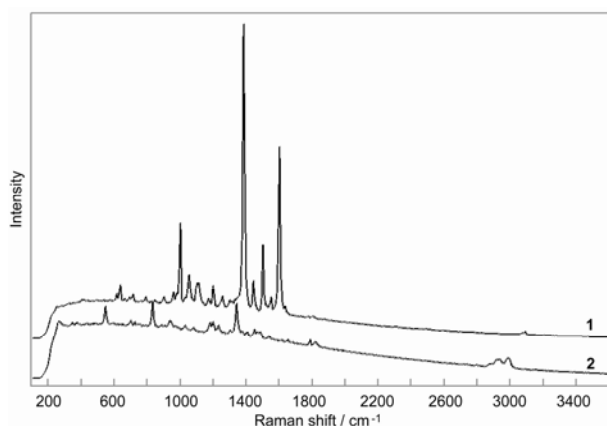

Fig. 6. Uncorrected Raman spectra of [C$_6$H$_5$C(O)CHC(O)C$_6$H$_5$](O$_2$CCO$_2$)B (**1**), [(CH$_3$)$_3$CCOCHCOC(CH$_3$)$_3$](O$_2$CCO$_2$)B (**2**)
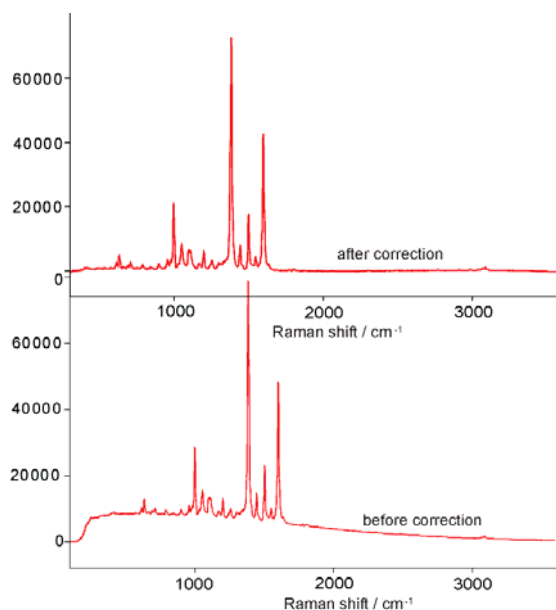
Fig. 7. The Raman spectrum of [C$_6$H$_5$C(O)CHC(O)C$_6$H$_5$](O$_2$CCO$_2$)B (**1**) before (lower spectrum) and after (upper spectrum) baseline correction

The normal modes of the aromatic C−H stretchings appear at lower frequencies. There are only two bands of small intensity in the Raman and several bands in the IR spectrum. Five pairs of

bands at almost the same energy are predicted to appear in the IR and Raman spectrum of **1**. They correspond to the vibrations of the separate phenyl rings and they are of almost the same energy. One has to bear in mind that the individual components of the pairs must be of different symmetry, otherwise resonance effects (Fermi resonance, for example) will cause the bands to split. Under C_{2v} point group symmetry the modes will belong to either A_1 or B_2 symmetry species. The local symmetry of **1** can also be confirmed by the fact that there is no splitting of the five bands that appear in the IR spectrum of **1**. It is interesting to note the positions of the maxima in the IR and in the Raman spectrum of **1**. Immediately follows that the in-phase mode makes up the intensity of the Raman band and the out-of-phase component the intensity of the IR band. The small difference (~ 6 cm^{-1}) suggests that the correlation field splitting is very small in the crystal of **1** or at least has not much influence to the vibrations of the phenyl C−H groups.

In the case of **2** the vinyl C−H stretch is split in two components, one at 3144 and other at 3156 cm^{-1}, which is clearly seen in both IR and Raman spectra of **2**. In the region of the CH$_3$ stretching modes of the *t*-butyl groups 9 pairs of modes are theoretically predicted. These bands are consisted of the in- and out-of-phase stretching modes for the two *t*-butyl groups, which are degenerate in energy. In the IR spectrum five broad bands are observed with no splitting of the individual pairs (the bands have almost no intensity in the Raman spectrum of **2**). The splitting of the vinyl C−H stretch might be due to the presence of two different C−H lengths in the unit cell of **2**.

The C=O stretching modes of the oxalate part of the spiroboron compound **1** appear at around 1800 cm^{-1}. Two bands due to in-phase and out-of-phase stretching modes of A_1 and B_1 symmetry are predicted to appear in the IR and Raman spectra with frequency difference of approximately 25 cm^{-1}. In the IR spectrum there are at least three bands in this region. After careful band reconstruction using a non-linear least squares fitting technique, it can be seen that there are four and three bands in the IR and Raman spectra, respectively. The number of bands under the band profiles in the experimental spectra is clear after examining the second derivative of the band envelope. The fitted results from the Raman spectrum should be taken with caution because of the low S/N ratio of

the experimental data and consequently the large error. The intensities of these bands in the Raman spectra are very low and the fitting will be less accurate. The frequency differences between the pairs of the peaks in the IR spectrum are 17 cm^{-1} and 23 cm^{-1} respectively, and the difference between the in-phase and out-of-phase components are 25 cm^{-1} and 30 cm^{-1} respectively. The relative IR intensities between the split components are 1.3 and 1.2 and the intensity ratio of the sums of the split bands is 2, while the predicted IR relative intensity is 3. The predicted relative Raman activity ratio is 1.6 which agrees well with the experimental data. It should be bared in mind that these results may not be the best possible solution to the experimental data and that more than four bands can be fitted to the experimental band profile. The bandwidths of the fitted spectrum are also worth mentioning. Actually, one of the components has much greater bandwidth than the other but it has very small height; nevertheless, the relative intensity ratios are almost the same between the two pairs of split bands. Trials to fit the band profile with 6 components, yielded similar result, the inner components of the band complex having greater bandwidth than the outer components which are much sharper.

There could be several reasons which could lead to splitting of the in-phase and the out-of-phase C=O stretching bands of the oxalate part of **1**. It is possible that the splitting is a result of intramolecular interactions of a Fermi resonance type, as a result of interaction between second order transitions and the C=O stretching modes with the same symmetry. The Fermi resonance might be also responsible for the smaller intensity ratio (2) of the two modes than the predicted value (3), since they might "borrow" some of their intensity to the second harmonic modes they interact with. Other reason, which could lead to splitting of these bands might be the correlation field present in the unit cell of the crystal of **1**. Experiments with isotopically labelled oxygen atoms on the carbonyl group might give some insight into the possible reasons for the appearance of more than one band in this frequency region.

In the case of **2** there are also at least 3 bands in the region of the C=O stretching modes of the oxalate part of the complex. It is interesting to note that the intensities of the two higher frequency components are switched and have larger Raman intensities when compared to the corresponding

bands in the Raman spectrum of **1**. The possible reason for this intensity swap may be an interaction with a second harmonic of some of the lower frequency modes with a different intensity and at different frequency from the overtone which possibly interacts with the C=O stretchings in the case of **1**. The larger Raman intensity in the spectrum of **2** may be due to the different shapes of the polarisability tensors of **1** and **2**.

4. CONCLUSIONS

The solvothermal method provides a convenient and economically feasible access to single crystalline phases of (diphenylpropen-1,3-diolato)-(oxalato)boron (**1**) and similar strongly lasing spiroconjugated bis-chelated boron compounds. Model ab initio calculations were performed to obtain the equilibrium molecular geometries and the vibrational (infrared, Raman) spectra of isolated β-ketoboronates, [RC(O)CHC(O)R'](O$_2$CCO$_2$)B R = R' = Ph; R = R' = *t*-butyl; R = Me, R'= Ph and R = R' = 2-pyridyl) in the ground state. The molecular structures resemble the solid state data of **1** and similar boron systems. The calculations reveal at least two local potential energy minima for each compound: tetrahedral (sp^3) BO$_4$ or trigonal-planar (sp^2) BO$_3$ coordination of the boron atoms. The former isomeric forms are much more stable, it is very likely that they coincide with the global minima on the potential multidimensional surface and also represent the actual molecular structures in the solids, as demonstrated in the case of **1**. By analysis of the vibrational spectra of the *t*-butyl analogue, for which the trigonal coordination is most probable among the studied systems, it is shown that although such minimum is indeed possible, only the more stable tetrahedral form exists in the solid state. This, on the other hand, confirms that the differences in the colour exhibited by the di-*t*-butyl and the other compounds stems from the specific electronic structure of this compound, conditioned by the absence of aromatic ring substituents. This conclusion is additionally supported by the existence of similar colourless tetrahedral (methylethylpropen-1,3-diolato)(oxalato)boron for which the X-ray data revealed tetrahedral coordination. It is probable that the spiro-type electronic transitions of the (dialkylpropen-1,3-diolato)(oxalato)boron system occur but fall out of the visible range; additional computations of the first excited

singlet and triplet states of this system should be performed in the future to gain insight in these presumptions. The spectral analysis points out several modes that can serve as a vibrational criterion for distinction of the boron coordination type. The present results, nevertheless, open several questions to be considered in the future studies of the spiro-boron compounds: *a.* assessment of the theoretical method through higher-level theoretical computations of the structures with extension of the basis set, *b.* comparison with spectra recorded from diluted solution or species isolated in an inert matrix, and *c.* theoretical vibronic analysis of the relevant excited molecular states and computation of the fluorescence spectra.

REFERENCES

[1] (a) M. Maeda, *Laser dyes: Properties of organic compound for dye lasers*, New York: Academic Press, **1984**; (b) H. Zollinger, *Color chemistry: Synthesis, properties and applications of organic dyes and pigments*, Weinheim: VCH, **1987**.

[2] *Selected papers on dye lasers*, Bellingham, Washington: SPIE Optical Engineering Press, **1992**.

[3] Y. L. Chow, Y.-H. Zhang, M. X. Zheng, A. Rassat, Absorption and fluorescence properties of tetracoordinated borates: energy versus electron transfer in spirointeractions, *Chem. Phys. Lett.* **272**, 471–477 (1997).

[4] V. E. Karasev, O. A. Korotkikh, Luminescence Properties of Boron β-Diketonates, *Russ. J. Inorg. Chem.* **30**, 1290–1292 (1985).

[5] P. Rapta, K. Erentova, A. Staško, H. Hartmann, Anion radicals as intermediates in the cathodic reduction of β-diketobornoates (cyclic voltammery, EPR and UV-VIS), *Electrochim. Acta* **39**, 2251–2259 (1994).

[6] (a) H. C. Lim, *Crystal structures and lasing characteristics of β-diketoboronates*, M. Tech. dissertation, University of Malaya, **1999**. (b) H. Lim, S. Yap, T. Tou, S. W. Ng, Amplified spontaneous emissions from (oxalato)-(dibenzoylmethanato)boron, *Opt. Mater.* **27**, 1815–1818 (2005).

[7] H. Hartmann, Ein einfacher Weg zu neuartigen Borhaltigen Spiroverbindungen, *J. Prakt. Chem.,* **328**, 755–762 (1986).

[8] N. D. Economou, V. P. Papageorgiou, J. Kopf, Synthesis and molecular structure of (oxalato)(2,4-hexanedionato)boron(III), *Z. Kristallogr.* **187**, 55–61 (1989).

[9] A. T. Balaban, I. Haiduc, H. Höpfl, N. Farfán, R. Santillan, Spiroborates revisited. X-ray crystal and molecular structures of boron chelate compounds with tropolone and 1,3-diketones, *Main Group Met. Chem.* **19**, 385-–395 (1996).

[10] H. Höpfl, N. P. Hernández, S. R. Líma, R. Santillan, N. Farfán, X-ray crystallographic study of neutral boron chelates with β-diketones and tropolone, *Heteroatom Chem.* **9**, 359–368 (1998).

[11] R. Boese, R. Köster, M. Yalpani, M. The colour of chelates of boron. An X-ray structural investigation of bis(4-methylphenyl)boryl and 9-borabicyclo-[3.3.1]nonyl acetylacetonates, *Chem. Ber.* **118**, 670–675 (1985).

[12] F. A. Cotton, W. H. Isley, Structure of a novel tetrahedral boron complex, bis(acetato)(acetylacetonato)boron(III), $B(O_2CMe)_2(acac)$, **21**, 300–302 (1982).

[13] S. J. Rettig, J. Trotter, Structural studies of organoboron compounds. XII. Crystal and molecular structures of (acetylacetonate)diphenylboron and (tropolonato)diphenylboron, *Can. J. Chem.* **60**, 2957–2964 (1982).

[14] CS CHEM3D modeling package, CambridgeSoft Corporation, **1998**.

[15] M. J. S. Dewar, E. G. Zoebisch, E. F. Healy, J. J. P. Stewart, Development and use of quantum mechanical molecular models. 76. AM1: a new general purpose quantum mechanical molecular model, *J. Am. Chem. Soc.* **107**, 3209–3903 (1985).

[16] M. J. S. Dewar, C. H. Reynolds, An improved set of mndo parameters for sulfur, *J. Comp. Chem.* **2**, 140–143 (1986).

[17] M. J. Frisch, et al. GAUSSIAN94w (rev. B2), Gaussian Inc., Pittsburgh PA, **1995**.

[18] M. J. Frisch, et al., GAUSSIAN98, Gaussian, Inc., Pittsburgh PA, **1998**.

[19] H. B. Schlegel, Optimization of equilibrium geometries and transition structures, *J. Comp. Chem.* **3**, 214–218 (1982).

[20] H. B. Schlegel, in *New theoretical Concepts for Understanding organic reactions*, Ed. J. Bertran, Kluwer Academic, The Netherlands, 33, **1989**.

[21] H. B. Schlegel, *Geometry Optimization on Potential Energy Surfaces*, in *Modern Electronic Structure Theory*, Ed. D. R. Yarkony, World Scientific Publishing, Singapore, **1994**.

[22] J. R. Durig, M. J. Lee, H. M. Badawi, J. F. Sullivan, D. I. Durig, Some applications of *ab initio* calculations in molecular spectroscopy, *J. Mol. Struct.* **266**, 59–64 (1992).

[23] I. G. Binev, B. A. Stamboliyska, Y. I. Binev, E. A. Velcheva, J. A. Tsenov, IR spectra and structure of 1-H-isoindole-1,3(2H)-dione (phthalimide), *cis*-hexahydro-1-H-isoindole-1,3(2H)-dione (hexahydrophthalimide) and of their nitranions, *J. Mol. Struct.* **513**, 231–243 (1999).

[24] B. A. Stamboliyska, Y. I. Binev, V. B. Radomirska, J. A. Tsenov, I. N. Juchnovski, IR spectra and structure of 2,5-pyrrolidinedione (succinimide) and of its nitranion: experimental and ab initio MO studies, *J. Mol. Struct.* **516**, 237–245 (2000).

[25] L. Lapinski, H. Rostkowska, M. J. Nowak, J. S. Kwiatkowski, J. Leszczynski, Infrared spectra of thiouracils: experimental matrix isolation and ab initio Hartree-Fock,

post-Hartree-Fock and density functional theory studies, *Vib. Spectrosc*. **13**, 23–40 (1996).

[26] B. A. Hess, L. J. Schaad, P. Čársky, R. Zahradník, Ab initio calculations of vibrational spectra and their use in the identification of unusual molecules, *Chem. Rev*. **86**, 709–730 (1986).

[27] A. D. Becke, Density-functional thermochemistry. III. The role of exact exchange, *J. Chem. Phys*. **98**, 5648–5652 (1993).

[28] C. Lee, W. Yang, R. G. Parr, Development of the Colle-Salvetti correlation-energy formula into a functional of the electron density, *Phys. Rev*. **B37**, 785–789 (1988).

[29] C. Møller, M. S. Plesset, Note on an Approximation Treatment for Many-Electron Systems, *Phys. Rev*. **46**, 618–622 (1934).

[30] R. S. Mülliken, Electronic Population Analysis on LCAO–MO Molecular Wave Functions, **23**, 1833–1840 (1955).

[31] N. N. Grenwood, *The Chemistry of Boron*, Oxford: Pergamon Press, Oxford, **1973**, pp. 906−909.

[32] R. H. Cragg, Other Aspects of Boron Chemistry, in *MTP International Review of Science, Inorganic Chemistry,* Ed. M.F. Lappert, Butterwords, London, **1972**.

[33] S. J. Rettig, J. Trotter, Crystal and Molecular Structure of *B,B*-Diphenylboroxazolidine (2-Aminoethyl Diphenyl-borinate), $Ph_2BO(CH_2)_2NH_2$, *Can. J. Chem*. **51**, 1288–1294 (1973).

[34] S. J. Rettig, J. Trotter, The crystal and molecular structure of *B,B*-bis-(*p*-fluorophenyl)boroxazolidine, $(p\text{-}FC_6H_4)_2BO(CH_2)_2NH_2$, *Acta Cryst*. **B30**, 2139–2145 (1974).

[35] S. J. Rettig, J. Trotter, Crystal and molecular structure of (salicylaldehydato)diphenylboron, *Can. J. Chem*. **54**, 1168–1175 (1976).

[36] H. Höpfl, M. Sánchez, V. Barba, N. Farfán, S. Rojas, R. Santillan, Synthesis and Study of Monomeric and Dimeric Boronates by Spectroscopic Methods and X-ray Crystallography, *Inorg. Chem*. **37**, 1679–1692 (1998).

[37] A. W. Hanson, E. W. Macaulay, The crystal structure of benzoylacetonato boron difluoride, *Acta Cryst*. **B28** 1961–1967 (1972).

[38] I. G. Binev, Infrared spectra and structure of butyldimethylammonium dicyanomethylide: an ab initio force field treatment, *Spectrochim. Acta* **A53**, 1795–1801 (1997).

[39] J. Fulara, M. J. Nowak, L. Lapinski, A. Les, L. Adamowicz, Theoretical and matrix-isolation experimental study of the infrared spectra of 5-azauracil and 6-azauracil, *Spectrochim. Acta* **A47**, 595–613 (1991).

[40] M. J. Nowak, A. Les, L. Adamowicz, Application of ab initio quantum mechanical calculations to assign matrix-isolation IR Spectra of oxopyrimidines, *Trends Phys. Chem*. **4**, 137–141 (1994).

[41] P. T. McKittirick, J. E. Katon, Infrared and Raman group frequencies of cyclic imides, *Appl. Spectrosc*. **44**, 812–817 (1990).

[42] R. A. Nyquist, S. L. Fiedler, Infrared study of five- and six-membered type cyclic imides, *Vib. Spectrosc*. **8**, 365–386 (1995).

[43] R. R. Servoss, H. M. Clark, Vibrational spectra of normal and isotopically labeled boric acid*, J. Chem. Phys*. **26**, 1175–1178 (1957).

[44] A. Meller, M. Wojnowska, (BO)-Banden in den IR-Spektren von Deuteroalkoxyboranen und Halogenalkoxy-boranen, *Monatsh. Chem*. **100**, 1489–1493 (1969).

[45] K. Wu, S.-Y. Lee, Ab initio calculations on normal mode vibrations and the Raman and IR spectra of the $[B_3O_6]^{3-}$ metaborate ring, *J. Phys. Chem*. **101**, 937–940 (1997).

[46] B. N. Meera, A. K. Sood, N. Chandrabhas, J. Ramakrishna, Raman study of lead borate glasses, *J. Non-Cryst. Solids* **126**, 224-230 (1990).

[47] D. Maniu, I. Ardelean, T. Iliescu, S. Cinta, O. Cozar, Raman spectroscopic investigations of the oxide glass system $(1-x)(3B_2O_3 \cdot K_2O)xMO$ (MO = V_2O_5 or CuO), *J. Mol. Struct*. **410/411**, 291–294 (1997).

[48] G. V. Kalacheva, E. Svarcs, V. G. Ben'kovskii, I. D. Lesnov, Borates, *Zh. Neorg. Khim*. **15**, 401–404 (1970).

[49] D. V. Lanzisera, L. Andrews, Reactions of laser-ablated boron atoms with methanol – Infrared spectra and ab initio calculations of CH_3BO, CH_2BOH, and CH_2BO in solid argon, *J. Phys. Chem*. **101**, 1482–1487 (1997).